PERGAMON

International Journal of Solids and Structures 36 (1999) 5399–5424

INTERNATIONAL JOURNAL OF SOLIDS and STRUCTURES

www.elsevier.com/locate/ijsolstr

A shell finite element for large strain elastoplasticity with anisotropies—Part I: Shell theory and variational principle

B. Schieck[a], W.M. Smoleński[b], H. Stumpf[b,*]

[a] *Fachhochschule Lübeck, Fachbereich M + W, D-23562 Lübeck, Germany*
[b] *Lehrstuhl für Allgemeine Mechanik, Ruhr-Universität Bochum, D-44780 Bochum, Germany*

Received 5 January 1998; in revised form 5 August 1998

Abstract

A shell model for finite elastic and finite plastic strains is derived taking into account initial and induced anisotropies. A corresponding eight-node C^0 shell element with three displacement and three director degrees-of-freedom at each node is developed, which combines the advantages of an isoparametric description of geometry and deformation with an effective plane stress formulation. The element accounts for isochoric or approximately isochoric deformation due to finite plastic strains. Because of the three displacement and three director degrees-of-freedom at each node, it is easily possible to link different parts of a composed irregular shell structure or to connect the derived shell element with solid (brick) elements.

This paper presents the shell theory based on the kinematics of finite elastoplasticity proposed in Schieck and Stumpf (1995) and the special geometric concept of the derived shell model. The Lagrange multiplier method is applied to introduce into the virtual work principle the transverse normality constraint and the condition of isochoric deformation, where the Lagrange multipliers can be condensed inside the element procedure. Various assumed strain techniques designed to avoid the membrane locking are compared with known methods in the literature. According to the numerical experience so far the proposed shell finite element is free of locking effects and spurious modes.

Part II presents the constitutive equations for finite elastic–plastic strains accounting for initial and induced anisotropies and the implementation of the model into the FE-code. A comprehensive set of numerical examples is provided, involving the tension of a plane specimen with necking and shear-band localization, the elastic–plastic response of a simply supported plate with a localization of the plastic bending strains in the four corner zones, the elastic–plastic deformation mode of the so-called Scordelis-Lo roof, and the elastic–plastic buckling of a cylindrical shell showing an essential influence of the anisotropic material behavior. The results illustrate the performance of the proposed shell finite element for a wide range of engineering applications.

* Corresponding author. Tel.: 00 49 234 70 06 025; fax: 00 49 234 70 94 154; e-mail: stumpf@am.bi.ruhr-uni-bochum.de

0020-7683/99/$ - see front matter
PII: S0020-7683(98)00254-6

1. Introduction

While in the late seventies and eighties nonlinear shell theories were investigated taking into account finite rotations but small strains (e.g. Pietraszkiewicz, 1984, 1989; Nolte et al., 1986; Valid, 1986; Başar and Krätzig, 1989; Gruttmann et al., 1989; Başar and Ding, 1990; Başar et al., 1992; Büchter and Ramm, 1992; Sansour and Bufler, 1992), main research efforts in the analysis of shells during the last couple of years were devoted to finite strain models. Shell theories for finite elastic strains were considered in Simmonds (1985, 1986), Stumpf and Makowski (1986), Makowski and Stumpf (1989, 1990) and Schieck et al. (1992). In the latter paper using a relaxed Kirchhoff–Love assumption accounting for the thickness change due to isochoric deformation of rubber-like materials, an arbitrarily shaped C^1 shell element for finite elastic strains was presented and applied to analyse numerically various finite elastic strain problems.

The needs of engineers call for the development of easily applicable isoparametric C^0 shell elements. Most of them are four-node flat quadrilateral elements and therefore, they approximate a curved shell as a facet structure. Bathe and Dvorkin (1986), Huang and Hinton (1986), and Huang (1987a, b) proposed numerical techniques known as 'assumed strain' methods, which can solve the problems of membrane and shear locking in four-, eight- and nine-node quadrilateral shell elements. Their propositions were applied since then by many authors within the range of small strain deformations. Simo et al. (1990) developed an isoparametric stress resultant four-node shell element for finite deformations. The kinematics is based on a director model and accounts also for the through-the-thickness stretching, what is typically needed for all shells with large strains. Chroscielewski et al. (1992, 1997) presented four-, nine- and 16-node quadrilateral isoparametric six-parameter C^0 shell elements based on a genuinely stress resultant formulation, which is also capable to deal with large strains. Recently, Başar and Ding (1997) presented a four-node five-parameter isoparametric shell element for deformations with large elastic strains. Their approach uses a director model, Euler angles for the rotation of the director, and accounts for the thickness change as a dependent property due to the isochoric behavior of rubber-like materials.

Elastic–plastic shell models for small strains were proposed by Schmidt and Weichert (1989) within a moderate rotation range and by Başar and Weichert (1991) for finite rotations. Both theories are based on an additive decomposition of the total strains into elastic and plastic parts, what is possible only within the small strain range. Associated finite elements were not given. Brank et al. (1997) developed a four-node isoparametric element for finite rotations and small elastic–plastic strains with isotropic hardening.

Based on the multiplicative decomposition of the total deformation gradient into elastic and plastic parts according to Bilby et al. (1955), Kröner (1960), and Lee (1969), Simo and Ortiz (1985) and Simo (1988) presented a framework for finite elastoplasticity using Lie derivatives as objective rates. The corresponding thermodynamics was considered by Le and Stumpf (1993), and a generalization of the model for elastic and induced plastic anisotropies was given by Miehe (1998a). Schieck and Stumpf (1995) proposed an alternative model of finite strain elastoplasticity based on a multiplicative decomposition of the total deformation gradient into Lagrangian and Eulerian, respectively, elastic and plastic stretches and a uniquely defined rotation tensor using the spin of this rotation tensor to construct the associated corotational rate.

Applying the Simo and Ortiz (1985) and Simo (1988) concept of finite elastoplasticity, Simo and Kennedy (1992) developed a shell finite element for large elastic–plastic deformation without

taking into account the change of the shell thickness caused by volume-preserving large plastic deformations. The element is restricted to isotropic material behavior. Stumpf and Schieck (1994) proposed a shell theory for finite elastic and finite plastic strains, where the kinematics is based on a relaxed Kirchhoff–Love hypothesis allowing transverse normal materials fibers to be stretched and bent, whereas shear deformations are neglected. Logarithmic membrane and bending strain measures were introduced to enable an additive decomposition for superposed moderately large strains (see also Schieck and Stumpf, 1993). An associated shell finite element was not given. The Simo concept of finite elastoplasticity was applied also by Roehl and Ramm (1996) to analyse shell problems for small elastic and large plastic strains and isotropic material behavior using various finite elements. For shells made of viscoplastic material An and Kollmann (1996) derived a theory for finite deformations, and Rouainia and Perić (1998) presented theory and finite element applications for viscoplastic shells as well. Recently, Miehe (1998b) presented a eight-node brick-type mixed finite shell element for large elastic–plastic deformations and isotropic material behavior. Several numerical examples were given for small elastic and large plastic strains.

The aim of this paper organized in two parts is to present a shell theory and a C^0 shell finite element for the analysis of shells undergoing finite elastic and finite plastic strains taking into account initial and induced anisotropies. The underlying concept of finite elastoplasticity is the one published in Schieck and Stumpf (1995). Essential features and advantages of the derived shell finite element are as follows:

- To our best knowledge it is the first shell element for combined large elastic and large plastic strains accounting for elastic and plastic anisotropies.
- It is a six-parameter shell model with three displacement degrees-of-freedom and three independent director degrees-of-freedom per node. Designed as an arbitrarily curved isoparametric eight-node shell element it approximates curved structures better than faced-like four-node elements.
- Shear and volume (change of thickness) locking is avoided by application of the Lagrange multiplier technique for the normality constraint of the director orientation and for the director length constraint due to (approximately) isochoric deformation. The Lagrange multipliers can be condensed inside the element procedure yielding numerically a pure displacement element.
- The membrane locking is overcome by application of assumed membrane strains that are fitted to the strains computed from the displacements by the least square method. Full numerical integration is applied. Thus, no interpolation between more or less heuristically chosen sampling points is needed. Numerical investigations show the improved performance compared with commonly used methods.
- The coupling with brick elements is easy and reliable, because the motion of a point at the upper or lower surface is a linear combination of the displacement of a node at the mid-surface and the 'deformation' of its director. This allows us to connect easily stiffeners with the shell, too.
- The coupling of parts of folded or multi shell structures can be achieved by prescribing the angles between the directors, e.g. realized as constraints controlled by Lagrange multipliers. In the range of really large strains this seems to be more reliable than the use of rotation tensors or vectors, because the rotation of a boundary line differs from the rotation of the material, if the membrane shear deformations parallel to the boundary are large.
- All tensors are given in Cartesian components referred to a material attached Cartesian coor-

dinate system. This is achieved by considering the Jacobian matrix of the isoparametric description of the element geometry as a fictitious deformation gradient due to a fictitious deformation from a flat rectangular reference configuration to the undeformed initial configuration. Therefore, the polar decomposition theorem can be applied on the fictitious deformation gradient, which is the Jacobian matrix, and the Cartesian reference frame can be rotated with the material into the undeformed configuration. One can consider the components of tensors that are referred to the rotated Cartesian reference as 'convective Cartesian' (cC) components.

- The application of tensors in cC-components enables an efficient plane stress description valid also in the thin shell limit.
- The description of tensors in cC components allows us to apply back-rotated Lagrangian type objective Cauchy or Kirchhoff stresses that are easily accessible for engineers, who want to formulate and implement refined material models with initial and induced elastic and plastic anisotropies, anisotropic yield conditions and flow rules.
- The concept has a well defined interface to enable the easy implementation of other material models.

This paper is organized as follows: in Section 2 we first recall the kinematics of finite elastoplasticity based on the multiplicative decompositions of the total deformation gradient into Lagrangian and Eulerian, respectively, elastic and plastic stretches and a uniquely defined rotation tensor. The kinematical concept is then generalized by introducing a second reference configuration with an additional fictitious deformation gradient, which allows us to refer the initial undeformed and all actual shell configurations to a flat rectangular plate with Cartesian reference frames. In Section 3 the kinematics of the shell finite element is established. In Section 4 we consider the virtual work principle as basis for the construction of the shell finite element and in Section 5 the associated Lagrange multipliers. In Section 6 assumed strain techniques are investigated and finally, in Section 7, the results of linear and nonlinear convergence tests are presented.

In Part II the constitutive model with back-rotated Kirchhoff stresses, the elastic–plastic return algorithm for finite strains and the numerical implementation will be discussed. The presented shell finite element will be applied to analyse a comprehensive set of numerical examples as plane bars with strain localization and necking, a plate with bending strain localization at the four corner zones, a cylindrical shell with two zones of bending strain localization and the elastic–plastic buckling of a cylinder under torsion with anisotropic material behavior.

2. Kinematics of finite elastoplasticity with respect to the initial undeformed and an additional reference configuration

In this section, we first recall some basic kinematic relations of finite elastoplasticity according to the constitutive model of Schieck and Stumpf (1995), and then we generalize the kinematics by introducing an additional reference configuration, which is an appropriate tool to construct an efficient shell finite element for large elastic and large plastic strains with initial and induced anisotropies. The kinematics is based on the multiplicative decomposition of the total deformation gradient into elastic and plastic parts, but constructed in such a way as to overcome the non-uniqueness of this decomposition.

According to Bilby et al. (1995), Kröner (1960), and Lee (1969) the total deformation gradient $\mathbf{F}$ can be decomposed into an elastic, $\mathbf{F}^e$, and a plastic, $\mathbf{F}^p$, contribution

$$\mathbf{F} = \mathbf{F}^e\mathbf{F}^p, \tag{2.1}$$

where $\mathbf{F}^e$ and $\mathbf{F}^p$ are incompatible point functions. Applying the polar decomposition theorem to $\mathbf{F}^e$ and $\mathbf{F}^p$ and indicating stretches referred to the intermediate configuration by a bar we have

$$\mathbf{F}^e = \mathbf{R}^e\bar{\mathbf{U}}^e = \mathbf{V}^e\mathbf{R}^e, \quad \mathbf{F}^p = \mathbf{R}^p\mathbf{U}^p = \bar{\mathbf{V}}^p\mathbf{R}^p, \tag{2.2}$$

where $\mathbf{R}^e$ and $\mathbf{R}^p$ are the elastic and plastic rotations, and $\bar{\mathbf{U}}^e$, $\mathbf{V}^e$ and $\mathbf{U}^p$, $\bar{\mathbf{V}}^p$ the elastic and plastic, respectively, right and left stretch tensors. Introducing (2.2) into (2.1) and defining the Lagrangian elastic stretch $\mathbf{U}^e$, the Eulerian plastic stretch $\mathbf{V}^p$, and the composed rotation tensor $\mathbf{Q}$ by

$$\mathbf{U}^e := \mathbf{R}^{pT}\bar{\mathbf{U}}^e\mathbf{R}^p = \mathbf{Q}^T\mathbf{V}^e\mathbf{Q}, \quad \mathbf{V}^p := \mathbf{Q}\mathbf{U}^p\mathbf{Q}^T, \quad \mathbf{Q} = \mathbf{R}^e\mathbf{R}^p, \tag{2.3}$$

we obtain the following two multiplicative decompositions,

$$\mathbf{F} = \mathbf{Q}\mathbf{U}^e\mathbf{U}^p = \mathbf{V}^e\mathbf{V}^p\mathbf{Q}, \tag{2.4}$$

alternative to the Bilby–Körner–Lee decomposition (2.1). Within a model of finite elastoplasticity, where constitutive and evolution laws are formulated for symmetric strain and stretch measures, respectively, the decompositions (2.4) are unique, contrary to (2.1). Of course, within such a model the rotation tensor $\mathbf{Q}$ cannot be split uniquely into elastic and plastic rotations according to $(2.3)_3$, but this is not needed for the corresponding corotational rate formulation.

Using $(2.4)_1$ the total right stretch tensor $\mathbf{U}$, following from the right polar decomposition $\mathbf{F} = \mathbf{R}\mathbf{U}$, can be decomposed into Lagrangian elastic, $\mathbf{U}^e$, and plastic, $\mathbf{U}^p$, stretches,

$$\mathbf{U} = \sqrt{\mathbf{F}^T\mathbf{F}} = \sqrt{\mathbf{U}^p\mathbf{U}^{e2}\mathbf{U}^p}, \tag{2.5}$$

from which the Lagrangian elastic stretch can be computed:

$$\mathbf{U}^e = \sqrt{\mathbf{U}^{p-1}\mathbf{U}^2\mathbf{U}^{p-1}}. \tag{2.6}$$

Thus, $\mathbf{U}^e$ is independent of the actual value of the plastic rotation $\mathbf{R}^p$ and depends only on the Lagrangian total stretch $\mathbf{U}$ and the Lagrangian plastic stretch $\mathbf{U}^p$. Correspondingly, from $(2.4)_2$ we derive the Eulerian decomposition of the total left stretch tensor $\mathbf{V}$ following from the left polar decomposition $\mathbf{F} = \mathbf{V}\mathbf{R}$,

$$\mathbf{V} = \sqrt{\mathbf{F}\mathbf{F}^T} = \sqrt{\mathbf{V}^e\mathbf{V}^{p2}\mathbf{V}^e}, \tag{2.7}$$

which allows us to determine the Eulerian plastic stretch tensor $\mathbf{V}^p$ from the Eulerian total stretch $\mathbf{V}$ and the Eulerian elastic stretch $\mathbf{V}^e$:

$$\mathbf{V}^p = \sqrt{\mathbf{V}^{e-1}\mathbf{V}^2\mathbf{V}^{e-1}}. \tag{2.8}$$

From (2.6) and (2.8) it follows that the multiplicative decompositions (2.4) are unique. It is easy to prove that $\mathbf{U}^e$ and $\mathbf{U}^p$ are Lagrangian objective and $\mathbf{V}^e$ and $\mathbf{V}^p$ Eulerian objective.

Let us denote the Kirchhoff stress tensor referred to the actual configuration by $\boldsymbol{\tau}$ and the corresponding back-stress tensor describing the kinematical hardening of the material by $\boldsymbol{\alpha}$. Then

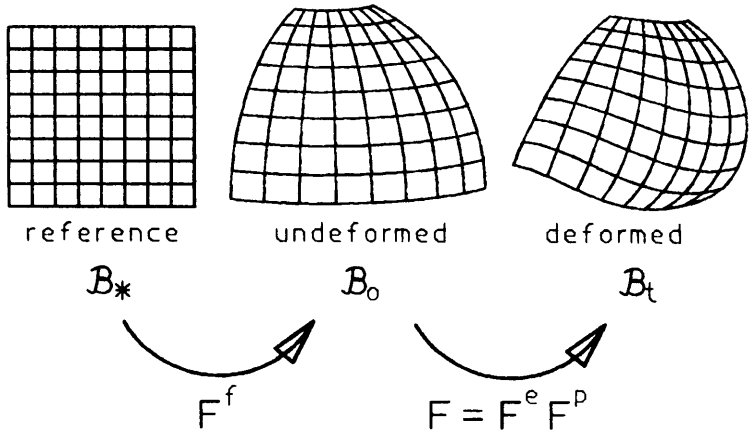

Fig. 1. Reference, undeformed and actual configurations of the shell.

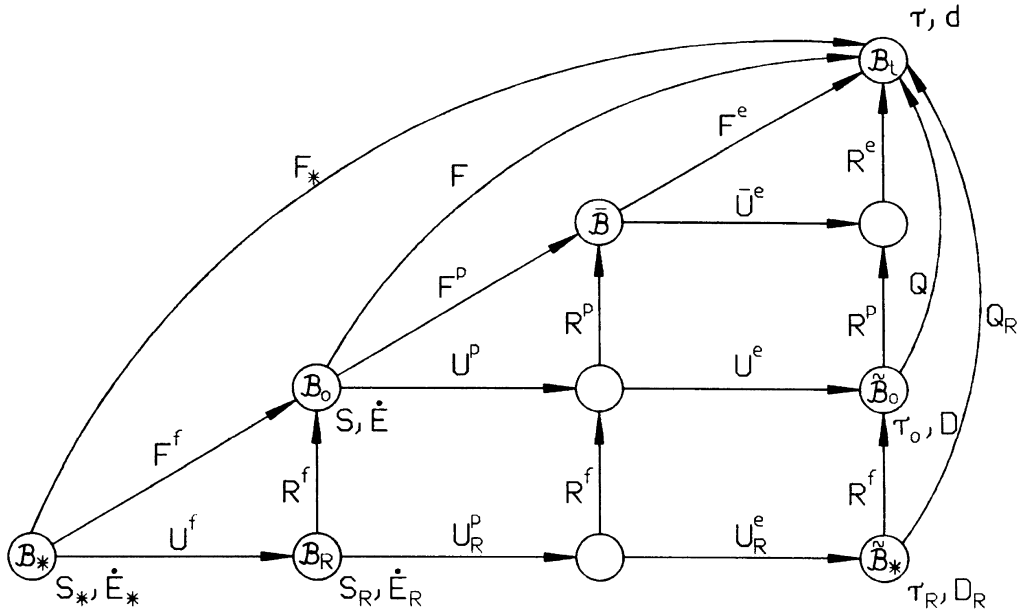

Fig. 2. Polar decompositions of the various deformation gradients and references of power-conjugate variables.

we can define Lagrangian objective Kirchhoff stresses $\boldsymbol{\tau}_0$ and back-stresses $\boldsymbol{\alpha}_0$ referred to $\tilde{\mathscr{B}}_0$ (see Fig. 2) by pull-back with $\mathbf{Q}$,

$$\boldsymbol{\tau}_0 = \mathbf{Q}^{\mathrm{T}}\boldsymbol{\tau}\mathbf{Q}, \quad \boldsymbol{\alpha}_0 = \mathbf{Q}^{\mathrm{T}}\boldsymbol{\alpha}\mathbf{Q}. \tag{2.9}$$

The corresponding constitutive equations will be considered in Part II of this paper.

In the above derived equations we refer stretches and stresses either to the initial undeformed configuration $\mathscr{B}_0$ or to the actual configuration $\mathscr{B}_t$. To construct an appropriate shell finite element

for finite elastic and finite plastic strains and to be able to use the plane stress assumption, we introduce now an additional reference configuration $\mathscr{B}_*$ such that the fictitious deformation gradient $\mathbf{F}^{\mathrm{f}}$ maps locally $\mathscr{B}_*$ into the initial, undeformed configuration $\mathscr{B}_0$. Then, the composed deformation gradient $\mathbf{F}_*$,

$$\mathbf{F}_* = \mathbf{F}\mathbf{F}^{\mathrm{f}} = \mathbf{F}^{\mathrm{e}}\mathbf{F}^{\mathrm{p}}\mathbf{F}^{\mathrm{f}}, \tag{2.10}$$

maps locally the new reference configuration $\mathscr{B}_*$ into the actual configuration $\mathscr{B}_{\mathrm{t}}$. This enables us to use an idea of Simo and Fox (1989) and to introduce a flat rectangular plate with local Cartesian reference frames (Fig. 1) as new reference configuration $\mathscr{B}_*$ for an appropriate shell analysis.

By this procedure we can refer all Lagrangian- and Eulerian-type tensors to Cartesian coordinates of the new reference configuration $\mathscr{B}_*$, what gives the tensor components a direct physical meaning and avoids the use of Christoffel symbols. Then, the tensor calculus of the shell theory reduces to simple matrix computations simplifying the programming work. The linear map $\mathbf{F}^{\mathrm{f}}$ needs to be compatible inside each element only, provided the configuration $\mathscr{B}_0$ of the undeformed shell is compatible as a whole. Thus, the shell finite element to be constructed has much in common with an isoparametric element, however with the difference that the Jacobian matrix is now treated as the fictitious deformation gradient $\mathbf{F}^{\mathrm{f}}$. Applying the polar decomposition theorem $\mathbf{F}^{\mathrm{f}} = \mathbf{R}^{\mathrm{f}}\mathbf{U}^{\mathrm{f}}$, we can determine the fictitious initial rotation $\mathbf{R}^{\mathrm{f}}$ and the fictitious initial stretch $\mathbf{U}^{\mathrm{f}}$. The fictitious initial rotation $\mathbf{R}^{\mathrm{f}}$ allows one to rotate all tensors back to the material attached flat rectangular reference configuration $\mathscr{B}_*$, what is the main difference to the common isoparametric formulation, and it enables us to use the plane stress assumption in the shell element. The kinematics of finite elastoplasticity generalized by the introduction of the new reference configuration $\mathscr{B}_*$ is sketched in Fig. 2.

First, we apply the polar decomposition theorem to the fictitious deformation gradient $\mathbf{F}^{\mathrm{f}}$ and obtain

$$\mathbf{F}^{\mathrm{f}} = \mathbf{R}^{\mathrm{f}}\mathbf{U}^{\mathrm{f}} = \mathbf{V}^{\mathrm{f}}\mathbf{R}^{\mathrm{f}}. \tag{2.11}$$

Corresponding to the eqns (2.3) we define the following stretch and rotation tensors,

$$\mathbf{U}_{\mathrm{R}}^{\mathrm{e}} := \mathbf{R}^{\mathrm{f}\mathrm{T}}\mathbf{U}^{\mathrm{e}}\mathbf{R}^{\mathrm{f}} = \mathbf{Q}_{\mathrm{R}}^{\mathrm{T}}\mathbf{V}^{\mathrm{e}}\mathbf{Q}_{\mathrm{R}}, \quad \mathbf{U}_{\mathrm{R}}^{\mathrm{p}} := \mathbf{Q}_{\mathrm{R}}^{\mathrm{T}}\mathbf{V}^{\mathrm{p}}\mathbf{Q}_{\mathrm{R}}, \quad \mathbf{Q}_{\mathrm{R}} := \mathbf{R}^{\mathrm{e}}\mathbf{R}^{\mathrm{p}}\mathbf{R}^{\mathrm{f}}. \tag{2.12}$$

With (2.11) and (2.12) we obtain the right and left decompositions of $\mathbf{F}_*$

$$\mathbf{F}_* = \mathbf{Q}_{\mathrm{R}}\mathbf{U}_{\mathrm{R}}^{\mathrm{e}}\mathbf{U}_{\mathrm{R}}^{\mathrm{p}}\mathbf{U}^{\mathrm{f}} = \mathbf{V}^{\mathrm{e}}\mathbf{V}^{\mathrm{p}}\mathbf{V}^{\mathrm{f}}\mathbf{Q}_{\mathrm{R}}, \tag{2.13}$$

which is the generalization of the decompositions (2.4) of finite elastoplasticity with one reference configuration. Corresponding to (2.5) and (2.7) we derive the decompositions of the 'total' stretches $\mathbf{U}_*$ and $\mathbf{V}_*$,

$$\begin{aligned} \mathbf{U}_* &= \sqrt{\mathbf{F}_*^{\mathrm{T}}\mathbf{F}_*} = \sqrt{\mathbf{U}^{\mathrm{f}}\mathbf{U}_{\mathrm{R}}^{\mathrm{p}}\mathbf{U}_{\mathrm{R}}^{\mathrm{e}2}\mathbf{U}_{\mathrm{R}}^{\mathrm{p}}\mathbf{U}^{\mathrm{f}}}, \\ \mathbf{V}_* &= \sqrt{\mathbf{F}_*\mathbf{F}_*^{\mathrm{T}}} = \sqrt{\mathbf{V}^{\mathrm{e}}\mathbf{V}^{\mathrm{p}}\mathbf{V}^{\mathrm{f}2}\mathbf{V}^{\mathrm{p}}\mathbf{V}^{\mathrm{e}}}. \end{aligned} \tag{2.14}$$

It can be proved easily (see e.g. Ogden, 1984) that all stretch tensors $\mathbf{V}$ are Eulerian objective and all stretch tensors $\mathbf{U}$ are Lagrangian objective (unaffected by superposed rigid-body motion).

In the kinematical picture of finite elastoplasticity with the undeformed reference configuration $\mathscr{B}_0$ we defined by (2.9) Lagrangian objective Kirchhoff stresses referred to $\tilde{\mathscr{B}}_0$. Correspondingly,

introducing the second reference configuration $\mathscr{B}_*$ we have to pull-back $\boldsymbol{\tau}_0$ and $\boldsymbol{\alpha}_0$ of eqns (2.9) by $\mathbf{R}^{\mathrm{f}}$ leading to the objective stress measures

$$\boldsymbol{\tau}_{\mathrm{R}} = \mathbf{R}^{\mathrm{fT}}\boldsymbol{\tau}_0\mathbf{R}^{\mathrm{f}} = \mathbf{Q}_{\mathrm{R}}^{\mathrm{T}}\boldsymbol{\tau}\mathbf{Q}_{\mathrm{R}}, \quad \boldsymbol{\alpha}_{\mathrm{R}} = \mathbf{R}^{\mathrm{fT}}\boldsymbol{\alpha}_0\mathbf{R}^{\mathrm{f}} = \mathbf{Q}_{\mathrm{R}}^{\mathrm{T}}\boldsymbol{\alpha}\mathbf{Q}_{\mathrm{R}}. \tag{2.15}$$

Corresponding second Piola–Kirchhoff type stresses $\mathbf{S}_*$ and back-stresses $\mathbf{A}_*$ referred to the second reference configuration $\mathscr{B}_*$ can be defined by

$$\begin{aligned}\mathbf{S}_* &= \mathbf{F}_*^{-1}\boldsymbol{\tau}\mathbf{F}_*^{-\mathrm{T}} = \mathbf{U}^{\mathrm{f}-1}\mathbf{U}_{\mathrm{R}}^{\mathrm{p}-1}\mathbf{U}_{\mathrm{R}}^{\mathrm{e}-1}\boldsymbol{\tau}_{\mathrm{R}}\mathbf{U}_{\mathrm{R}}^{\mathrm{e}-1}\mathbf{U}_{\mathrm{R}}^{\mathrm{p}-1}\mathbf{U}^{\mathrm{f}-1},\\ \mathbf{A} &= \mathbf{F}_*^{-1}\mathbf{A}\mathbf{F}_*^{-\mathrm{T}} = \mathbf{U}^{\mathrm{f}-1}\mathbf{U}_{\mathrm{R}}^{\mathrm{p}-1}\mathbf{U}_{\mathrm{R}}^{\mathrm{e}-1}\boldsymbol{\alpha}_{\mathrm{R}}\mathbf{U}_{\mathrm{R}}^{\mathrm{e}-1}\mathbf{U}_{\mathrm{R}}^{\mathrm{p}-1}\mathbf{U}^{\mathrm{f}-1}.\end{aligned} \tag{2.16}$$

Another useful set of second Piola–Kirchhoff type stresses is defined by (see Fig. 2)

$$\begin{aligned}\mathbf{S}_{\mathrm{R}} &= \mathbf{U}_{\mathrm{R}}^{\mathrm{p}-1}\mathbf{U}_{\mathrm{R}}^{\mathrm{e}-1}\boldsymbol{\tau}_{\mathrm{R}}\mathbf{U}_{\mathrm{R}}^{\mathrm{e}-1}\mathbf{U}_{\mathrm{R}}^{\mathrm{p}-1} = \mathbf{U}^{\mathrm{f}}\mathbf{S}_*\mathbf{U}^{\mathrm{f}}\\ \mathbf{A}_{\mathrm{R}} &= \mathbf{U}_{\mathrm{R}}^{\mathrm{p}-1}\mathbf{U}_{\mathrm{R}}^{\mathrm{e}-1}\boldsymbol{\alpha}_{\mathrm{R}}\mathbf{U}_{\mathrm{R}}^{\mathrm{e}-1}\mathbf{U}_{\mathrm{R}}^{\mathrm{p}-1} = \mathbf{U}^{\mathrm{f}}\mathbf{A}_*\mathbf{U}^{\mathrm{f}}.\end{aligned} \tag{2.17}$$

To formulate the virtual work principle we have to define the power-conjugate strain rates. Power-conjugate to the Kirchhoff stress tensor $\boldsymbol{\tau}$ is the Eulerian deformation rate $\mathbf{d}$,

$$\mathbf{d} = \tfrac{1}{2}(\dot{\mathbf{F}}_*\mathbf{F}_*^{-1} + \mathbf{F}_*^{-\mathrm{T}}\dot{\mathbf{F}}_*^{\mathrm{T}}) = \tfrac{1}{2}(\dot{\mathbf{F}}\mathbf{F}^{-1} + \mathbf{F}^{-\mathrm{T}}\dot{\mathbf{F}}^{\mathrm{T}}), \tag{2.18}$$

where we have taken into account that $\mathbf{F}^{\mathrm{f}}$ is time-independent. The strain rates associated with the Kirchhoff stress tensor (2.15), the second Piola–Kirchhoff stress tensors (2.16) and (2.17) are

$$\mathbf{D}_{\mathrm{R}} = \mathbf{Q}_{\mathrm{R}}^{\mathrm{T}}\mathbf{d}\mathbf{Q}_{\mathrm{R}} = \mathbf{U}_{\mathrm{R}}^{\mathrm{e}-1}\mathbf{U}_{\mathrm{R}}^{\mathrm{p}-1}\mathbf{U}_{\mathrm{R}}^{\mathrm{f}-1}\dot{\mathbf{E}}_*\mathbf{U}_{\mathrm{R}}^{\mathrm{f}-1}\mathbf{U}_{\mathrm{R}}^{\mathrm{p}-1}\mathbf{U}_{\mathbf{R}}^{\mathrm{e}-1}, \tag{2.19}$$

$$\dot{\mathbf{E}}_* = \tfrac{1}{2}(\dot{\mathbf{F}}_*^{\mathrm{T}}\mathbf{F}_* + \mathbf{F}_*^{\mathrm{T}}\dot{\mathbf{F}}_*) = \mathbf{F}_*^{\mathrm{T}}\mathbf{d}\mathbf{F}_* \tag{2.20}$$

$$\dot{\mathbf{E}}_{\mathrm{R}} = \mathbf{U}_{\mathrm{R}}^{\mathrm{p}}\mathbf{U}_{\mathrm{R}}^{\mathrm{e}}\mathbf{D}_{\mathrm{R}}\mathbf{U}_{\mathrm{R}}^{\mathrm{e}}\mathbf{U}_{\mathrm{R}}^{\mathrm{p}} = \mathbf{U}^{\mathrm{f}-1}\dot{\mathbf{E}}_*\mathbf{U}^{\mathrm{f}-1} = \mathbf{Q}^{\mathrm{fT}}\mathbf{F}^{\mathrm{T}}\mathbf{d}\mathbf{F}\mathbf{Q}^{\mathrm{f}}, \tag{2.21}$$

where (2.21) is the rate of the Green-type strain tensor $\mathbf{E}_{\mathrm{R}}$ referred to the back-rotated undeformed configuration $\mathscr{B}_{\mathrm{R}}$ (see Fig. 2),

$$\mathbf{E}_{\mathrm{R}} = \mathbf{R}^{\mathrm{fT}}\tfrac{1}{2}(\mathbf{F}^{\mathrm{T}}\mathbf{F} - \mathbf{1})\mathbf{R}^{\mathrm{f}} = \mathbf{U}^{\mathrm{f}-1}\tfrac{1}{2}(\mathbf{F}_*^{\mathrm{T}}\mathbf{F}_* - \mathbf{F}^{\mathrm{fT}}\mathbf{F}^{\mathrm{f}})\mathbf{U}^{\mathrm{f}-1}. \tag{2.22}$$

The corresponding right stretch tensor $\mathbf{U}_{\mathrm{R}} = (\mathbf{1} + 2\mathbf{E}_{\mathrm{R}})^{1/2}$, following from back-rotation with $\mathbf{R}^{\mathrm{f}}$ of the stretch tensor $\mathbf{U}$ according to (2.5), has an elastic plastic decomposition as follows:

$$\mathbf{U}_{\mathrm{R}} = \mathbf{R}^{\mathrm{fT}}\mathbf{U}\mathbf{R}^{\mathrm{f}} = \sqrt{\mathbf{U}_{\mathrm{R}}^{\mathrm{p}}\mathbf{U}_{\mathrm{R}}^{\mathrm{e}2}\mathbf{U}_{\mathbf{R}}^{\mathrm{p}}}. \tag{2.23}$$

With the above derived stresses and corresponding strain and strain rates, respectively, we have introduced a set of Lagrangian objective variables that describe the stress state and the deformation of the shell in a material configuration with local Cartesian coordinates, and we are able to use a plane stress state to analyse arbitrary shells undergoing finite elastic–plastic strains. Also due to the Cartesian reference, the formulation of constitutive equations does not require essential knowledge of modern tensor calculus, which makes this work easily accessible to engineers.

3. Kinematics of the shell element

The kinematics of the shell element consists of three mid-surface displacement components and three director components as basic kinematical unknowns. The position vector of any material point $\mathbf{X}(X^\alpha, \zeta)$, $\alpha \in \{1, 2\}$, $\zeta \equiv X^3$, in the flat, rectangular reference configuration $\mathscr{B}_*$ of the shell space is given by

$$\mathbf{X}(X^\alpha, \zeta) = X^1\mathbf{e}_1 + X^2\mathbf{e}_2 + \zeta\mathbf{e}_3 = \mathbf{X}(X^\alpha, 0) + \zeta\mathbf{T}(X^\alpha), \tag{3.1}$$

where $\mathbf{e}_1$, $\mathbf{e}_2$, $\mathbf{e}_3$ are Cartesian base vectors in the reference configuration with $\mathbf{e}_3 \equiv \mathbf{T}$ as the director on the mid-surface. With H we denote the thickness of the shell in the Cartesian reference configuration $\mathscr{B}_*$, and $\zeta \in [-H/2, H/2]$ is the corresponding coordinate. In the undeformed configuration $\mathscr{B}_0$ the position vector becomes

$$\mathbf{x}_0(X^\alpha, \zeta) = \mathbf{x}_0(X^\alpha, 0) + \zeta\mathbf{t}_0(X^\alpha) \tag{3.2}$$

with $\mathbf{t}_0$ as undeformed director. The director length $|\mathbf{t}_0|$ is given by the ratio of the thickness h_0 of the undeformed shell to the reference thickness H: $|\mathbf{t}_0| = h_0/H$. If one assumes the transformation from the reference configuration $\mathscr{B}_*$ into the undeformed configuration $\mathscr{B}_0$ to be isochoric and transverse orthogonal, $|\mathbf{t}_0|$ is given by $H/h_0 = 1/|\mathbf{t}_0| = |\partial/\partial X^1\mathbf{x}_{0|\zeta=0} \times \partial/\partial X^2\mathbf{x}_{0|\zeta=0}|$. In the actual configuration the position vector becomes

$$\mathbf{x}(X^\alpha, \zeta) = \mathbf{x}(X^\alpha, 0) + \zeta\mathbf{t}(X^\alpha) \tag{3.3}$$

with $\mathbf{t}$ as the actual director. From (3.1)–(3.3) the 'total' displacement field $\mathbf{u}_*$ and the physically real displacement field $\mathbf{u}$ are obtained as

$$\mathbf{u}_*(X^\alpha, \zeta) = \mathbf{x}(X^\alpha, 0) - \mathbf{X}(X^\alpha, 0) + \zeta(\mathbf{t}(X^\alpha) - \mathbf{T}(X^\alpha)) \tag{3.4}$$

and

$$\mathbf{u}(X^\alpha, \zeta) = \mathbf{v}(X^\alpha, 0) + \zeta(\mathbf{t}(X^\alpha) - \mathbf{t}_0(X^\alpha)). \tag{3.5}$$

In order to ensure high accuracy also in the small deformation limit, the real physical mid-surface displacement

$$\mathbf{v}(X^\alpha) = \mathbf{x}(X^\alpha, 0) - \mathbf{x}_0(X^\alpha, 0) \tag{3.6}$$

and the real physical director difference ('displacement') $\mathbf{t}(X^\alpha) - \mathbf{t}_0(X^\alpha)$ must be introduced instead of $\mathbf{x}(X^\alpha, 0)$ and $\mathbf{t}(X^\alpha)$ as primary unknowns. Analogously, we define the fictitious 'initial displacement' $\mathbf{v}_\mathrm{f}$ of the undeformed configuration ratio by

$$\mathbf{v}_\mathrm{f}(X^\alpha) = \mathbf{x}_0(X^\alpha, 0) - \mathbf{X}(X^\alpha, 0). \tag{3.7}$$

In the chosen eight-node shell element each node has three degrees-of-freedom for each of the displacements $\mathbf{v}$ and $\mathbf{v}_\mathrm{f}$ of the mid-surface and three degrees-of-freedom for each of the director differences $\mathbf{t} - \mathbf{t}_0$ and $\mathbf{t}_0 - \mathbf{T}$. The mid-surface displacements are interpolated in the usual manner with bi-quadratic shape functions. They are complete up to the quadratic order, what is important for the performance of the element, and additionally they have some cubic terms. For the director differences $\mathbf{t} - \mathbf{t}_0$ and $\mathbf{t}_0 - \mathbf{T}$, we apply a more refined interpolation in order to enable both, high

accuracy in the case of bending deformations with distorted meshes and the calculation of discrete jumps of $\mathbf{t}_0$ and $\mathbf{t}$ due to jumps of the shell reference thickness H in the reference configuration $\mathscr{B}_*$ but with continuous true thickness. For this purpose we define the normalized director differences

$$\mathbf{t}' = \frac{H}{h_0}(\mathbf{t}-\mathbf{t}_0) \quad \text{and} \quad \mathbf{t}_0' = \frac{H}{h_0}(\mathbf{t}_0-\mathbf{T}). \tag{3.8}$$

They are interpolated in the usual manner with bi-quadratic shape functions like the mid-surface displacements. The distribution of the ratio H/h_0 between the nine Gaussian quadrature points of the element is approximated by bi-quadratic interpolation, too. Then $\nabla(\mathbf{t}-\mathbf{t}_0)$ and $\nabla(\mathbf{t}_0-\mathbf{T}) \equiv \nabla\mathbf{t}_0$, needed in the sequel, become

$$\nabla(\mathbf{t}-\mathbf{t}_0) = \frac{h_0}{H}\nabla\mathbf{t}' + \mathbf{t}' \otimes \nabla\left(\frac{h_0}{H}\right), \quad \nabla\mathbf{t}_0 = \frac{h_0}{H}\nabla\mathbf{t}_0' + \mathbf{t}_0' \otimes \nabla\left(\frac{h_0}{H}\right), \tag{3.9}$$

where $\nabla(h_0/H)$ can be obtained from the interpolation of H/h_0 as $\nabla(h_0/H) = -(h_0/H)^2\nabla(H/h_0)$. However, since eqns (3.9) are applied only in eqn (3.13) for $\mathbf{X}_R$ and derived variables, one can show that the underlined terms do not contribute to $\mathbf{X}_R$ and its derivatives, if transverse orthogonality is taken into account. Therefore, in the finite element program code they can be omitted.

The orthogonality condition of the directors and the control of the director length due to (approximately) isochoric deformation are introduced as constraints into the variational principle with the help of Lagrange multipliers, which will be outlined in the next section. This leads to additional degrees of freedom in the nodal points of the shell element. However, as it will also be discussed in the next section, it is possible to eliminate them on element level. By this procedure the element is reduced to a pure displacement element, which makes its introduction into standard finite element program packages possible.

From the 'plane' deformation gradients

$$\mathbf{F}^{\mathrm{f}} = \frac{\partial\mathbf{x}_0}{\partial X^\alpha} \otimes \mathbf{e}_\alpha = \nabla\mathbf{x}_0(X^\alpha, 0) + \zeta\nabla\mathbf{t}_0(X^\alpha) = \mathbf{1} + \nabla\mathbf{v}_{\mathrm{f}} + \zeta\nabla\mathbf{t}_0 \tag{3.10}$$

and

$$\mathbf{F}_* = \frac{\partial\mathbf{x}}{\partial X^\alpha} \otimes \mathbf{e}_\alpha = \mathbf{1} + \nabla\mathbf{v}_{\mathrm{f}} + \nabla\mathbf{v} + \zeta\nabla\mathbf{t}, \tag{3.11}$$

the plane Green strain tensor $\mathbf{E}_R$ referred to the configuration $\mathscr{B}_R$ (see Fig. 2) can be calculated according to eqn $(2.22)_2$, yielding

$$\begin{aligned}\mathbf{E}_R = \tfrac{1}{2}\mathbf{U}^{\mathrm{f}-1}[&(\nabla\mathbf{v}^{\mathrm{T}} + \zeta\nabla(\mathbf{t}-\mathbf{t}_0)^{\mathrm{T}})(\mathbf{1} + \nabla\mathbf{v}_{\mathrm{f}} + \zeta\nabla\mathbf{t}_0) + (\mathbf{1} + \nabla\mathbf{v}_{\mathrm{f}}^{\mathrm{T}} + \zeta\nabla\mathbf{t}_0^{\mathrm{T}})(\nabla\mathbf{v} + \zeta\nabla(\mathbf{t}-\mathbf{t}_0)) \\ &+ (\nabla\mathbf{v}^{\mathrm{T}} + \zeta\nabla(\mathbf{t}-\mathbf{t}_0)^{\mathrm{T}})(\nabla\mathbf{v} + \zeta\nabla(\mathbf{t}-\mathbf{t}_0))]\mathbf{U}^{\mathrm{f}-1},\end{aligned} \tag{3.12}$$

where $\mathbf{U}^{\mathrm{f}} = (\mathbf{F}^{\mathrm{fT}}\mathbf{F}^{\mathrm{f}})^{1/2}$. By series expansion with respect to the ζ-coordinate the expression

$$\mathbf{E}_{\mathrm{R}} = \boldsymbol{\gamma}_{\mathrm{R}} + \zeta\boldsymbol{\chi}_{\mathrm{R}} + \text{higher-order terms} \tag{3.13}$$

can be obtained, where

$$\boldsymbol{\gamma}_{\mathrm{R}} = \mathbf{U}^{\mathrm{f}-1}_{(0)}\boldsymbol{\gamma}\mathbf{U}^{\mathrm{f}-1}_{(0)}, \quad \boldsymbol{\gamma} = \tfrac{1}{2}[\nabla\mathbf{v}^{\mathrm{T}}(\mathbf{1}+\nabla\mathbf{v}_{\mathrm{f}}) + (\mathbf{1}+\nabla\mathbf{v}_{\mathrm{f}}^{\mathrm{T}})\nabla\mathbf{v} + \nabla\mathbf{v}^{\mathrm{T}}\nabla\mathbf{v}] \tag{3.14}$$

denotes the Green membrane strain tensor, and

$$\begin{aligned}\boldsymbol{\chi}_{\mathrm{R}} = \tfrac{1}{2}\mathbf{U}^{\mathrm{f}-1}_{(0)}[&\nabla(\mathbf{t}-\mathbf{t}_0)^{\mathrm{T}}(\mathbf{1}+\nabla\mathbf{v}_{\mathrm{f}}) + (\mathbf{1}+\nabla\mathbf{v}_{\mathrm{f}}^{\mathrm{T}})\nabla(\mathbf{t}-\mathbf{t}_0)\\ &+\nabla\mathbf{v}^{\mathrm{T}}\nabla\mathbf{t} + \nabla\mathbf{t}^{\mathrm{T}}\nabla\mathbf{v} - 2\mathbf{U}^{\mathrm{f}}_{(1)}\mathbf{U}^{\mathrm{f}-1}_{(0)}\boldsymbol{\gamma} - 2\boldsymbol{\gamma}\mathbf{U}^{\mathrm{f}-1}_{(0)}\mathbf{U}^{\mathrm{f}}_{(1)}]\mathbf{U}^{\mathrm{f}-1}_{(0)}\end{aligned} \tag{3.15}$$

is the Green bending strain tensor. In the above equations

$$\mathbf{U}^{\mathrm{f}}_{(0)} := \mathbf{U}^{\mathrm{f}}_{|\zeta=0} = \sqrt{(\mathbf{1}+\nabla\mathbf{v}_{\mathrm{f}})^{\mathrm{T}}(\mathbf{1}+\nabla\mathbf{v}_{\mathrm{f}})} \tag{3.16}$$

stands for the fictitious 'initial stretch' of the mid-surface and $\mathbf{U}^{\mathrm{f}}_{(1)} := \partial\mathbf{U}^{\mathrm{f}}/\partial\zeta_{|\zeta=0}$ for the thickness derivative of the 'initial stretch' at the mid-surface. The latter one can be obtained solving the equation

$$\mathbf{U}^{\mathrm{f}}_{(0)}\mathbf{U}^{\mathrm{f}}_{(1)} + \mathbf{U}^{\mathrm{f}}_{(1)}\mathbf{U}^{\mathrm{f}}_{(0)} = (\mathbf{1}+\nabla\mathbf{v}_{\mathrm{f}}^{\mathrm{T}})\nabla\mathbf{t}_0 + \nabla\mathbf{t}_0^{\mathrm{T}}(\mathbf{1}+\nabla\mathbf{v}_{\mathrm{f}}) \tag{3.17}$$

for $\mathbf{U}^{\mathrm{f}}_{(1)}$. Due to the estimations in Schieck and Stumpf (1994) the higher-order terms in the series expansion of the strain distribution (3.13) with respect to the thickness direction can be neglected.

For the derivation of the incremental form of the internal virtual work the first variations, $\delta\boldsymbol{\gamma}_{\mathrm{R}}$, $\delta\boldsymbol{\chi}_{\mathrm{R}}$, and the second variations, $\Delta\delta\boldsymbol{\gamma}_{\mathrm{R}}$, $\Delta\delta\boldsymbol{\chi}_{\mathrm{R}}$, of $\boldsymbol{\gamma}_{\mathrm{R}}$ and $\boldsymbol{\chi}_{\mathrm{R}}$ are needed. With Δ and δ denoting independent variations due to independent virtual changes of the deformation and director deformation fields, we obtain

$$\delta\boldsymbol{\gamma}_{\mathrm{R}} = \mathbf{U}^{\mathrm{f}-1}_{(0)}\delta\boldsymbol{\gamma}\mathbf{U}^{\mathrm{f}-1}_{(0)} \tag{3.18}_1$$

with

$$\delta\boldsymbol{\gamma} = \tfrac{1}{2}(\delta\nabla\mathbf{v}^{\mathrm{T}}(\mathbf{1}+\nabla\mathbf{v}_{\mathrm{f}}) + (\mathbf{1}+\nabla\mathbf{v}_{\mathrm{f}}^{\mathrm{T}})\delta\nabla\mathbf{v} + \delta\nabla\mathbf{v}^{\mathrm{T}}\nabla\mathbf{v} + \nabla\mathbf{v}^{\mathrm{T}}\delta\nabla\mathbf{v}),$$

$$\delta\boldsymbol{\chi}_{\mathrm{R}} = \tfrac{1}{2}\mathbf{U}^{\mathrm{f}-1}_{(0)}(\delta\nabla\mathbf{t}^{\mathrm{T}}(\mathbf{1}+\nabla\mathbf{v}_{\mathrm{f}}) + (\mathbf{1}+\nabla\mathbf{v}_{\mathrm{f}}^{\mathrm{T}})\delta\nabla\mathbf{t} + \delta\nabla\mathbf{v}^{\mathrm{T}}\nabla\mathbf{t} + \nabla\mathbf{v}^{\mathrm{T}}\delta\nabla\mathbf{t} + \nabla\mathbf{t}^{\mathrm{T}}\delta\nabla\mathbf{v} + \delta\nabla\mathbf{t}^{\mathrm{T}}\nabla\mathbf{v} \tag{3.18}_2$$

$$-2\mathbf{U}^{\mathrm{f}}_{(1)}\mathbf{U}^{\mathrm{f}-1}_{(0)}\delta\boldsymbol{\gamma} - 2\delta\boldsymbol{\gamma}\mathbf{U}^{\mathrm{f}-1}_{(0)}\mathbf{U}^{\mathrm{f}}_{(1)})\mathbf{U}^{\mathrm{f}-1}_{(0)}, \tag{3.19}$$

$$\Delta\delta\boldsymbol{\gamma}_{\mathrm{R}} = \mathbf{U}^{\mathrm{f}-1}_{(0)}\Delta\delta\boldsymbol{\gamma}\mathbf{U}^{\mathrm{f}-1}_{(0)} \quad \text{with } \Delta\delta\boldsymbol{\gamma} = \tfrac{1}{2}(\delta\nabla\mathbf{v}^{\mathrm{T}}\Delta\nabla\mathbf{v} + \Delta\nabla\mathbf{v}^{\mathrm{T}}\delta\nabla\mathbf{v}), \tag{3.20}$$

$$\begin{aligned}\Delta\delta\boldsymbol{\chi}_{\mathrm{R}} = \tfrac{1}{2}\mathbf{U}^{\mathrm{f}-1}_{(0)}(&\delta\nabla\mathbf{v}^{\mathrm{T}}\Delta\nabla\mathbf{t} + \Delta\nabla\mathbf{v}^{\mathrm{T}}\delta\nabla\mathbf{t} + \Delta\nabla\mathbf{t}^{\mathrm{T}}\delta\nabla\mathbf{v} + \delta\nabla\mathbf{t}^{\mathrm{T}}\Delta\nabla\mathbf{v}\\ &-2\mathbf{U}^{\mathrm{f}}_{(1)}\mathbf{U}^{\mathrm{f}-1}_{(0)}\Delta\delta\boldsymbol{\gamma} - 2\Delta\delta\boldsymbol{\gamma}\mathbf{U}^{\mathrm{f}-1}_{(0)}\mathbf{U}^{\mathrm{f}}_{(1)})\mathbf{U}^{\mathrm{f}-1}_{(0)}.\end{aligned} \tag{3.21}$$

The advantage of choosing $\mathbf{E}_{\mathrm{R}} = \boldsymbol{\gamma}_{\mathrm{R}} + \zeta\boldsymbol{\chi}_{\mathrm{R}}$ according to eqns (2.22) and (3.13) as strain measure in the shell referred to the back-rotated undeformed configuration $\mathscr{B}_{\mathrm{R}}$ instead of the Green strain measure $\mathbf{E} = \boldsymbol{\gamma} + \zeta\boldsymbol{\chi}$ referred to the real undeformed configuration $\mathscr{B}_0$ is the fact that the former enables the application of Cartesian tensor components and an effective plane stress description due to the local material-attached Cartesian reference frames.

4. Variational principle

As basis for the construction of the shell finite element the Lagrangian virtual work principle is used. We extend the internal virtual work by introducing the transverse normality constraint and the condition of isochoric deformation with the help of Lagrange multipliers. Then the total virtual work VW is composed of the internal virtual work IVW, the extensions XVW of the internal virtual work due to the Lagrange multiplier constraints, and the external virtual work EVW,

$$VW = IVW + XVW + EVW. \tag{4.1}$$

According to the virtual work principle the total virtual work VW vanishes for equilibrium states.

The internal virtual work density is given by the scalar product of a stress tensor with its power-conjugate objective strain rate, e.g. $\mathbf{S}\cdot\delta\mathbf{E} = \mathbf{S}_*\cdot\delta\mathbf{E}_* = \mathbf{S}_R\cdot\delta\mathbf{E}_R = \boldsymbol{\tau}\cdot\mathbf{d}(\delta\mathrm{F}) = \boldsymbol{\tau}_R\cdot\mathbf{D}(\delta\mathrm{F})_R$, where the index $(\delta\mathrm{F})$ of $\mathbf{d}$ and $\mathbf{D}$ denotes that they are computed from $\delta\mathbf{F}$ instead of $\dot{\mathbf{F}}$. In the incremental form one of the following equal valued expressions $\Delta\mathbf{S}\cdot\delta\mathbf{E} + \mathbf{S}\cdot\Delta\delta\mathbf{E} = \Delta\mathbf{S}_*\cdot\delta\mathbf{E}_* + \mathbf{S}_*\cdot\Delta\delta\mathbf{E}_* = \Delta\mathbf{S}_R\cdot\delta\mathbf{E}_R + \mathbf{S}_R\cdot\Delta\delta\mathbf{E}_R = \Delta\boldsymbol{\tau}\cdot\mathbf{d}(\delta\mathrm{F}) + \boldsymbol{\tau}\cdot\Delta\mathbf{d}(\delta\mathrm{F}) = \Delta\boldsymbol{\tau}_R\cdot\mathbf{D}(\delta\mathrm{F})_R + \boldsymbol{\tau}_R\cdot\Delta\mathbf{D}(\delta\mathrm{F})_R$ have to be calculated, where Δ denotes another variation of the deformation independent of the variation δ. If a Lagrangian form of the internal virtual work is chosen, e.g. $\mathbf{S}\cdot\delta\mathbf{E} = \mathbf{S}_*\cdot\delta\mathbf{E}_* = \mathbf{S}_R\cdot\delta\mathbf{E}_R = \boldsymbol{\tau}_R\cdot\mathbf{D}(\delta\mathrm{F})_R$ with Lagrangian objective tensors, the variations Δ of them can be calculated easily like a material time derivative. In the Eulerian form $\boldsymbol{\tau}\cdot\mathbf{d}(\delta\mathrm{F})$, $\Delta\boldsymbol{\tau}$ and $\Delta\mathbf{d}(\delta\mathrm{F})$ have to be computed as Lie-derivatives or as a co-rotational rate according to Schieck and Stumpf (1995).

In the following the Lagrangian form $\mathbf{S}_R\cdot\delta\mathbf{E}_R$ is chosen to represent the internal virtual work density. The reference configuration is then the back-rotated underformed configuration $\mathscr{B}_R$ (see Fig. 2). Since $\mathbf{U}^f$ is constant during the really physical deformation process, this configuration is a Lagrangian reference. The stresses $\mathscr{N}_R$ and stress couples $\mathscr{M}_R$, which are work-conjugate to $\delta\boldsymbol{\gamma}_R$ and $\delta\boldsymbol{\chi}_R$, are computed from $\mathbf{S}_R$ as

$$\mathscr{N}_R = \int_{-H/2}^{H/2} \mathbf{S}_R(\zeta)\,\mathrm{d}\zeta \tag{4.2}$$

and

$$\mathscr{M}_R = \int_{-H/2}^{H/2} \mathbf{S}_R(\zeta)\zeta\,\mathrm{d}\zeta, \tag{4.3}$$

where H is the shell thickness in the reference configuration $\mathscr{B}_*$. H can be obtained from the thickness in the undeformed configuration due to the condition, that the fictitious initial deformation with the gradient $\mathbf{F}^f$ is isochoric. Then IVW becomes

$$IVW = \int_V \mathbf{S}_R\cdot\delta\mathbf{E}_R\,\mathrm{d}V = \int_A (\mathscr{N}_R\cdot\delta\boldsymbol{\gamma}_R + \mathscr{M}_R\cdot\delta\boldsymbol{\chi}_R)\,\mathrm{d}A, \tag{4.4}$$

where A is the area of the mid-surface in the reference configuration $\mathscr{B}_*$.

The normality constraint, demanding the actual director $\mathbf{t}$ to be perpendicular to the mid-surface, is $\mathbf{t}\mathbf{F}_{*|\zeta=0} = \mathbf{0}$, because $\mathbf{F}_{*|\zeta=0}$ as the plane mid-surface gradient (3×2-matrix) contains the actual convective tangent vectors at the mid-surface. The isochoric constraint is $\det\mathbf{F}^{(3\times 3)}_{*|\zeta=0} = 1$, where $\mathbf{F}^{(3\times 3)}_{*|\zeta=0} = \mathbf{F}_{*|\zeta=0} + \mathbf{t}\otimes\mathbf{e}_3$ is the full three-dimensional deformation gradient at the mid-surface

with $\mathbf{e}_3$ as the Cartesian base vector in the third direction. In order to avoid residual stresses in the elements, which would disturb the computations with very small deformations, the normality constraint must be checked to $\mathbf{t}\mathbf{F}_{*|\zeta=0} = \mathbf{t}_0\mathbf{F}^{\mathrm{f}}_{|\zeta=0}$, because due to the continuity of the undeformed geometry of a finite element discretization, $\mathbf{t}_0\mathbf{F}^{\mathrm{f}}_{|\zeta=0}$ cannot be exactly zero in all integration points of all elements. Analogously, the isochoric constraint should be checked to $\det \mathbf{F}^{(3\times3)}_{*|\zeta=0} = \det \mathbf{F}^{\mathrm{f}(3\times3)}_{|\zeta=0}$, where $\mathbf{F}^{\mathrm{f}(3\times3)}_{|\zeta=0} = \mathbf{F}^{\mathrm{f}}_{|\zeta=0} + \mathbf{t}_0 \otimes \mathbf{e}_3$. Then the extensions to the virtual work principle are

$$\begin{aligned} XVW &= \int_A \delta[(\mathbf{t}\mathbf{F}_{*|\zeta=0} - \mathbf{t}_0\mathbf{F}^{\mathrm{f}}_{|\zeta=0})\cdot\boldsymbol{\lambda} + \eta(\det \mathbf{F}^{(3\times3)}_{*|\zeta=0} - \det \mathbf{F}^{\mathrm{f}(3\times3)}_{|\zeta=0})]\,\mathrm{d}A \\ &= \int_A [(\mathbf{t}\mathbf{F}_{*|\zeta=0} + \mathbf{t}_0\mathbf{F}^{\mathrm{f}}_{|\zeta=0})\cdot\delta\boldsymbol{\lambda} + \mathbf{t}\cdot\delta\nabla\mathbf{v}\cdot\boldsymbol{\lambda} - \delta\mathbf{t}\cdot\mathbf{F}_{*|\zeta=0}\cdot\boldsymbol{\lambda} \\ &\quad + \delta\eta(\det \mathbf{F}^{(3\times3)}_{*|\zeta=0} - \det \mathbf{F}^{\mathrm{f}(3\times3)}_{|\zeta=0}) + \eta\,\mathrm{tr}(\delta\mathbf{F}^{(3\times3)}_{*|\zeta=0}\mathbf{F}^{(3\times3)-1}_{*|\zeta=0})\det \mathbf{F}^{(3\times3)}_{*|\zeta=0}]\,\mathrm{d}A, \end{aligned} \tag{4.5}$$

where $\boldsymbol{\lambda}$ is the Lagrange multiplier vector that controls the transverse normality constraint, and η is the Lagrange multiplier that controls the change of the director length due to the incompressibility constraint. With $\delta\boldsymbol{\lambda}$ and $\delta\eta$ we denote the variations or virtual changes of $\boldsymbol{\lambda}$ and η.

Applying the Gaussian divergence theorem to $IVW + XVW$ one can see that $|\mathbf{t}|^2\mathbf{F}_{*|\zeta=0}\boldsymbol{\lambda}$ is the (approximated) Cauchy transverse shear force vector (in convective Cartesian components) and that η/H is a superposed hydrostatic pressure. The second Piola–Kirchhoff transverse shear force vector is obtained by pull-back as $|\mathbf{t}|\boldsymbol{\lambda}$. For small elastic transverse shear deformations the corresponding shear deformation energy is then

$$W_{\mathrm{shear}} = \int_a \frac{0.6}{Gh}\boldsymbol{\lambda}\cdot\mathbf{U}^2_{*(0)}\boldsymbol{\lambda}|\mathbf{t}|^4\,\mathrm{d}a = \int_A \frac{0.6}{GH}\,\boldsymbol{\lambda}\cdot\mathbf{U}^2_{*(0)}\boldsymbol{\lambda}|\mathbf{t}|^2\,\mathrm{d}A, \tag{4.6}$$

where $\mathbf{U}^2_{*(0)} = \mathbf{F}^{\mathrm{T}}_{*|\zeta=0}\mathbf{F}_{*|\zeta=0}$ is the squared 'total' stretch of the mid-surface and the covariant metric of the mid-surface, respectively. In (4.6) $\mathrm{d}a$ is the actual mid-surface area element, h the actual shell thickness and G the shear modulus. Additionally, we have $h/H = |\mathbf{t}| = \mathrm{d}A/\mathrm{d}a$, what holds exactly for isochoric deformations only, and shear correction factor of 1.2 has been taken into account. If for the condensation of $\boldsymbol{\lambda}$ some lower accuracy is acceptable, the transverse shear deformation energy can be approximated by

$$W_{\mathrm{shear}} \approx \int_A \frac{0.6}{GH}\boldsymbol{\lambda}\cdot\mathbf{U}^{\mathrm{f}2}_{(0)}\boldsymbol{\lambda}|\mathbf{t}_0|^2\,\mathrm{d}A. \tag{4.7}$$

According to the physical meaning of η, the bulk energy W_{bulk} for small elastic volume changes is

$$W_{\mathrm{bulk}} = \int_A \frac{\eta^2}{2E_{\mathrm{b}}H}\mathrm{d}A, \tag{4.8}$$

where E_{b} denotes the bulk modulus.

Introducing into the virtual work principle the variation of the negative transverse shear deformation energy and the variation of the negative bulk energy we obtain

$$VW = IVW + XVW - \delta W_{\text{shear}} - \delta W_{\text{bulk}} + EVW, \tag{4.9}$$

which leads to a virtual work expression of Hellinger–Reissner type. Herewith, the Lagrange multipliers can be considered as independent stress fields according to the previously derived physical meaning, and they can be condensed for a wide range of the parameters. Within this extension, transverse shear deformations for moderately thick shells are taken into account, which is appropriate for elastic shells. However, for elastic–plastic deformations and when the shell thickness increases to moderate size, this way of introducing the transverse shear stress and the corresponding shear deformation is not a real improvement, because this approach is unable to take into account the real distribution of the transverse shear stresses over the thickness and its disorder due to plastic flow. Therefore, the transverse shear stresses cannot be introduced into the yield condition appropriately. For thin shells this does not influence the results essentially because of the relatively small values of the transverse shear stresses.

The impossibility of a realistic modelling of transverse elastic–plastic shear deformations in a shell element is the reason, why the authors decided to exclude transverse shear deformations by the use of Lagrange multipliers. However, then one has to accept them as additional nodal degrees of freedom on the system level outside the element procedure, because their elimination on the element level reintroduces transverse shear deformations. Of course, instead of using Lagrange multipliers or mixed methods, one could also apply assumed strain techniques to avoid the shear locking.

After introducing the bulk energy into the variational principle, the shell finite element accounts also for moderately large changes of the volume due to moderately large non-isochoric elastic strains. Here, for plane stress material models an assumed strain technique is not possible.

Since the external virtual work of the present shell model does not differ from the common ansatz (see e.g. Stumpf and Schieck, 1994), it will not be considered here. Only the hydrostatic pressure load p needs some comment. To formulate the pressure load it was found that the application of the actual director $\mathbf{t}$ leads to a weak convergence ratio in the Newton–Raphson iterations. Therefore, it is preferable to use the following form

$$EVW_{\text{press}} = -\int_A p \left(\left.\frac{\partial \mathbf{x}}{\partial X^1}\right|_{\zeta=0} \times \left.\frac{\partial \mathbf{x}}{\partial X^2}\right|_{\zeta=0} \right) \cdot \delta \mathbf{v} \, \mathrm{d}A, \tag{4.10}$$

where $\partial \mathbf{x}/\partial X^1$, $\partial \mathbf{x}/\partial X^2$ are the actual convective tangent vectors included in the first two columns of the matrix $\mathbf{F}_*$. With a cross we denote the usual vector product of two vectors.

For the derivation of the stiffness matrix the incremental form of VW is needed. With Δ and δ denoting independent variations with respect to virtual changes of the deformation and Lagrange multipliers, the incremental total virtual work ΔVW becomes

$$\Delta VW = \Delta IVW + \Delta XVW - \Delta\delta W_{\text{shear}} - \Delta\delta W_{\text{bulk}} + \Delta EVW. \tag{4.11}$$

For dead loads, the incremental external virtual work ΔEVW vanishes and for ΔIVW and ΔXVW we obtain

$$\Delta IVW = \int_A (\Delta \mathscr{N}_{\mathrm{R}} \cdot \delta \boldsymbol{\gamma}_{\mathrm{R}} + \Delta \mathscr{M}_{\mathrm{R}} \cdot \delta \boldsymbol{\chi}_{\mathrm{R}} + \mathscr{N}_{\mathrm{R}} \cdot \Delta\delta \boldsymbol{\gamma}_{\mathrm{R}} + \mathscr{M}_{\mathrm{R}} \cdot \Delta\delta \boldsymbol{\chi}_{\mathrm{R}}) \, \mathrm{d}A, \tag{4.12}$$

and

$$\Delta XVW = \int_A \{(\Delta \mathbf{t}\mathbf{F}_{*|\zeta=0} + \mathbf{t}\Delta\nabla\mathbf{v})\cdot\delta\boldsymbol{\lambda} + (\delta\mathbf{t}\mathbf{F}_{*|\zeta=0} + \mathbf{t}\delta\nabla\mathbf{v})\cdot\Delta\boldsymbol{\lambda} + (\Delta\mathbf{t}\delta\nabla\mathbf{v} + \delta\mathbf{t}\Delta\nabla\mathbf{v})\cdot\boldsymbol{\lambda}$$
$$+ [\delta\eta\,\mathrm{tr}(\Delta\mathbf{F}^{(3\times3)}_{*|\zeta=0}\mathbf{F}^{(3\times3)-1}_{*|\zeta=0}) + \Delta\eta\,\mathrm{tr}(\delta\mathbf{F}^{(3\times3)}_{*|\zeta=0}\mathbf{F}^{(3\times3)-1}_{*|\zeta=0})]\det\mathbf{F}^{(3\times3)}_{*|\zeta=0}$$
$$+ \eta[\mathrm{tr}(\delta\mathbf{F}^{(3\times3)}_{*|\zeta=0}\mathbf{F}^{(3\times3)-1}_{*|\zeta=0})\,\mathrm{tr}(\Delta\mathbf{F}^{(3\times3)}_{*|\zeta=0}\mathbf{F}^{(3\times3)-1}_{*|\zeta=0})$$
$$- \mathrm{tr}(\delta\mathbf{F}^{(3\times3)}_{*|\zeta=0}\mathbf{F}^{(3\times3)-1}_{*|\zeta=0}\Delta\mathbf{F}^{(3\times3)}_{*|\zeta=0}\mathbf{F}^{(3\times3)-1}_{*|\zeta=0})\det\mathbf{F}^{(3\times3)}_{*|\zeta=0}]\}\,\mathrm{d}A. \tag{4.13}$$

The expressions for $\Delta\delta W_{\mathrm{shear}}$, $\Delta\delta W_{\mathrm{bulk}}$ and $\Delta EVW_{\mathrm{press}}$ are not presented here, because they can be calculated without problems.

5. Shape functions for the Lagrange multiplier fields

The shear locking is avoided by introducing the transverse normality constraint into the variation principle (4.1) and (4.5), receptively, with the help of a two-dimensional vector field $\boldsymbol{\lambda}$ as Lagrange multiplier. However, the trial functions for the components of $\boldsymbol{\lambda}$ should not have more degrees-of-freedom than the trial functions for the components of the director $\mathbf{t}$. Spurious modes of bending are circumvented, if the trial functions for $\boldsymbol{\lambda}$ have not less degrees-of-freedom than the gradient of the transverse mid-surface displacement field. Optimal flexibility is obtained, if one uses only the minimum number of degrees-of-freedom. According to the usual interpolation functions for geometry and displacements that are applied in the present eight-node shell element, the gradient of the transverse mid-surface displacement has eight degrees-of-freedom, which requires four degrees-of-freedom for each component of $\boldsymbol{\lambda}$. Since the first components of the mid-surface displacement gradient $\nabla\mathbf{v}$ are continuous over the element edges that are parallel to X^1, and the second components of $\nabla\mathbf{v}$ are continuous over the element edges that are parallel to X^2 (where X^1, X^2 are the element mid-surface coordinates, see Section 3), it is advisable to choose the same continuity for the corresponding Lagrange multiplier field $\boldsymbol{\lambda}$. This means that λ^1 is continuous over the element boundaries in the X^2-direction and λ^2 is continuous in the X^1 direction. This guarantees that there is always exactly the same number of degrees-of-freedom for $\boldsymbol{\lambda}$ and for components of the gradient of the transverse mid-surface displacement. This special continuity can easily be achieved, if the nodal degrees-of-freedom for λ^1 are placed in the mid-nodes of the edges parallel to X^1 and analogously those for λ^2 in the mid-nodes of the edges parallel to X^2.

Since, physically speaking, not $\boldsymbol{\lambda}$ but the second Piola–Kirchhoff shear force vector $|\mathbf{t}|\boldsymbol{\lambda} \equiv h/H\boldsymbol{\lambda}$ is continuous across the element boundaries, the numerical accuracy of the element can be increased, if one chooses the above mentioned interpolation and continuity for $\boldsymbol{\lambda}' := h_0/H\boldsymbol{\lambda}$. There, the continuity of $h/h_0 = |\mathbf{t}|/|\mathbf{t}_0|$ is taken into account with given C^0 continuity of the director field.

In order to avoid volume (or thickness) locking, the constraint of isochoric deformation is also introduced into the variational principle (4.1) and (4.5), respectively, using η as a Lagrange multiplier field. Since in each node the director length should be adjusted to the determinant of the mid-surface deformation gradient, each node gets the nodal value of η as an additional degree-of-freedom. In this way, there are always as many directors, the lengths of which must be adjusted, as there are Lagrange multipliers to achieve this. The interpolation function for η is the same as the one used for the displacement components and director displacements. Since η/H is the

superposed hydrostatic pressure, the numerical accuracy of the element can be increased, if one chooses $\eta' := \eta/H$ as nodal degree-of-freedom and also for the corresponding interpolation.

After introducing the shear deformation energy as outlined in Section 4 the condensation of $\boldsymbol{\lambda}$ on the element level is easy to implement. However, the condensation of η leads to stiffening effects for coarse element meshes. This can be circumvented, if for η a bi-linear interpolation instead of a bi-cubic interpolation is applied. In this case spurious modes in thickness changes can be avoided by introducing into the variational principle an additional energy term according to the gradient of the thickness change. An appropriate choice is

$$W_{\text{gradthick}} = \int k \frac{GH^3}{24\mathbf{t}_0 \cdot \mathbf{t}_0} (\mathbf{t}\nabla(\mathbf{t}-\mathbf{t}_0)) \cdot \mathbf{U}_{(0)}^{\mathrm{f}-2} \cdot (\mathbf{t}\nabla(\mathbf{t}-\mathbf{t}_0))\, \mathrm{d}A, \tag{5.1}$$

where k is a scaling factor. Due to our numerical experience it should be chosen between 0.01 and 0.5, where in most cases good results were obtained for $k = 0.1$.

6. Assumed membrane strains

In the shell finite element presented in this paper the membrane locking is avoided by applying assumed membrane strain fields. The most common approach is that of Bathe and Dvorkin (1986). However, in this and other related papers no theoretical background is given for the choice of the so-called sampling points used for the strain interpolation. Therefore, we investigate in this paper how to construct appropriately assumed strain fields and how to fit them to the strains computed 'exactly' from the deformations.

Membrane locking occurs only in curved thin-walled shell structures, and it is of practical significance in low-order elements. In elements with shape functions of fifth- or higher-order the locking plays no significant role. From the engineering point of view, the origin of membrane locking is the fact that because of the low-order approximation of the geometry of deformation the element is unable to perform membrane-strain-free bending modes. This causes us to construct and fit the assumed membrane strain fields so that the element can perform bending modes but without exhibiting spurious modes.

These remarks suggest that there must exist essential restrictions for the assumed membrane strain fields. As minimal requirement the assumed membrane strain field should have at least as many free parameters as the in-plane deformation field minus 3 in-plane rigid-body motions. For the present eight-node element this means 8×2 in-plane deformations minus 3 in-plane rigid-body motions, what makes a minimum of 13 free parameters for the assumed membrane strain field. The other bound is obtained from the requirement that the element should be able to perform some (at least two or three) membrane-strain-free bending modes. This implies the following calculation: eight nodes with three translatoric displacements minus 6 spatial rigid-body motions leads to 18 different deformation modes. Since two or, better, three modes should be without membrane strains, one obtains a maximum number of 16 or, better, 15 free parameters for the assumed membrane strain field.

In the present element the assumed strain approach is applied to the Green membrane strains $\boldsymbol{\gamma}$ defined in eqn $(3.14)_2$. These membrane strains are also present in the bending strain tensor (3.15).

The approach of Bathe and Dvorkin (1986), which is programmed in our FE-Code as one of various assumed strain techniques, has 16 free parameters, i.e. the strains in the sampling points for the interpolation of the assumed membrane strain field. Another approach is the one of Huang and Hinton (1986), which, applied to eight-node elements, has also 16 free parameters, i.e. the coefficients of the shape functions of the assumed strains. Again, the arrangement of sampling points plays an important role. However, the choice of number and position of the sampling points seems to be only due to the numerical experience of the authors in both approximation procedures. This was the reason for us to reconsider this problem.

One may ask, why a selective reduced integration of the membrane strain energy is not applied here. According to the authors experience, there is no reduced integration scheme known for the membrane energy that does not have instabilities like spurious modes, if no additional stabilization procedure is applied. This fact can easily be explained taking e.g. 2×2 point integration, as it is implemented in several commercial eight-node shell element codes. For this purpose let us consider an elastic flat sheet. Then one element has eight nodes times two in-plane deformations minus 3 in-plane rigid-body motions yielding 13 independent deformation modes. In the case of plane stress the deformation energy depends on the three independent components of the symmetric plane strain tensor. Using a 2×2 point integration the membrane energy of the element is computed from four nodes times three strain components yielding 12 scalar values. Thus, the deformation energies of the above mentioned 13 independent deformation modes are mapped on 12 scalars. The result is, that there is $1 = 13-12$ independent deformation modes that do not change the components of the strain tensor in any integration point. This is exactly the reason for a spurious mode.

As our first alternative procedure of assumed membrane strains we propose the following approach with 13 free parameters, a_1–a_5, b_1–b_5 and c_1–c_3:

$$\gamma^{\mathrm{as}}_{11}(X, Y) = a_1 + a_2 X + a_3 Y + a_4 XY + a_5 (Y)^2, \tag{6.1}$$

$$\gamma^{\mathrm{as}}_{22}(X, Y) = b_1 + b_2 X + b_3 Y + b_4 (X)^2 + b_5 XY, \tag{6.2}$$

$$\gamma^{\mathrm{as}}_{12}(X, Y) = c_1 + c_2 X + c_3 Y + \tfrac{1}{4} a_4 (X)^2 + (a_5 + b_4) XY + \tfrac{1}{4} b_5 (Y)^2. \tag{6.3}$$

Here, $X \equiv X^1$ and $Y \equiv X^2$ are the element mid-surface coordinates in the reference configuration and $\gamma^{\mathrm{as}}_{ij}$ are the components of the approximated field of the Green membrane strain tensor defined in eqn $(3.14)_2$. The fields for the components of the assumed strains are coupled as in the geometrically linear eight-node plane sheet element. The assumed strain field is fitted to the strain field computed from the displacements by a least square method using full numerical integration. This implies that the expression

$$\int_A (\boldsymbol{\gamma}^{\mathrm{as}} - \boldsymbol{\gamma}) \cdot \mathbb{C} \cdot (\boldsymbol{\gamma}^{\mathrm{as}} - \boldsymbol{\gamma})\, \mathrm{d}A \tag{6.4}$$

has to be minimized, where $\boldsymbol{\gamma}$ denotes the strains that are directly computed from the displacement field. Since expression (6.4) is a quadratic form, a constant transformation matrix between the computed strains $\boldsymbol{\gamma}$ and the assumed strains $\boldsymbol{\gamma}^{\mathrm{as}}$ in the integration points is obtained. For $\mathbb{C}$ the elasticity tensor or any other appropriate symmetric fourth-order tensor can be chosen, e.g. the fourth-order unity tensor.

As our second alternative procedure the assumed strain components γ_{11}^{as} and γ_{22}^{as} are taken as above, but γ_{12}^{as} is approximated now independently of γ_{11}^{as} and γ_{22}^{as} as

$$\gamma_{12}^{as}(X, Y) = c_1 + c_2 X + c_3 Y + c_4 XY. \tag{6.5}$$

This approach has 14 free parameters and has similarities with the strain distribution of Bathe and Dvorkin (1986). As in our first proposition the assumed strain field is fitted by the least square method.

7. Convergence tests

In order to demonstrate the performance of the proposed shell element, we present here the numerical results of the patch test, of the analysis of the thin hemispherical shell with hole according to MacNeal and Harder (1985) and of the moderately thin hemisphere of Simo and Kennedy (1992).

First, let us consider our results of the patch test proposed by MacNeal and Harder (1985) for membrane and bending deformations. The geometrical properties and boundary conditions are shown in Fig. 3. The results of the membrane patch test are given in Table 1. there one can see that without assumed strain technique, which is not needed for flat problems, the relative errors in the solution are zero (in a numerical sense). Applying assumed membrane strains there are numerical errors in the range of some percent. For the present element this is not surprising, because the strain tensor components are referred to material-, i.e. element-, attached convective Cartesian components, and the element geometry is nonlinear generating large in-plane rotations of the local Cartesian reference frames. Therefore, the assumed strain techniques cut off always

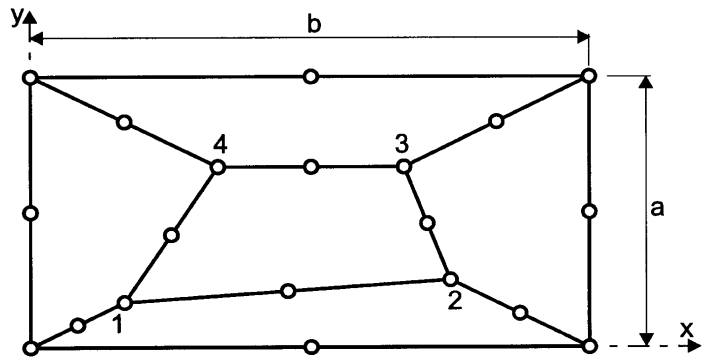

	x	y
1	0.04	0.02
2	0.18	0.03
3	0.16	0.08
4	0.08	0.08

a = 0.12, b = 0.24,
E = 10^6, ν = 0.25

Boundary conditions

membrane patch test:	bending patch test:
h = 0.001	$w = 10^{-3}(x^2 + xy + y^2)/2$
$u = 10^{-3}(x + y/2)$	$\theta_x = \partial w/\partial y = 10^{-3}(y + x/2)$
$v = 10^{-3}(y + x/2)$	$\theta_y = -\partial w/\partial x = 10^{-3}(-x - y/2)$

Fig. 3. Patch test: geometry and boundary conditions.

Table 1
Membrane patch test: maximum and averaged relative errors

Method	$\frac{\max \lvert\Delta\gamma_{RI}\rvert}{\gamma_{RI}}$	$\frac{\max \lvert\Delta\gamma_{RII}\rvert}{\gamma_{RI}}$	$\frac{\sqrt{\frac{1}{n}\sum_n \Delta\gamma_{RI}^2}}{\gamma_{RI}}$	$\frac{\sqrt{\frac{1}{n}\sum_n \Delta\gamma_{RII}^2}}{\gamma_{RI}}$
Without assumed strains	$7.769 \cdot 10^{-7}$	$2.905 \cdot 10^{-7}$	$7.497 \cdot 10^{-7}$	$2.481 \cdot 10^{-7}$
Method 2: 14 parameters	0.0361	0.0260	0.0120	0.0103
Bathe–Dvorkin method	0.0426	0.0431	0.0114	0.0163
Huang–Hinton method	0.0848	0.1710	0.0425	0.0519

Analytical principal membrane strains: $\gamma_{RI} = 0.0015$, $\gamma_{RII} = 0.0005$.

higher order contributions of the strain distribution, which are needed to gain the exact solution. It is interesting to see that the assumed strain method proposed by the authors produces smaller relative errors than the established methods of Bathe–Dvorkin and Huang–Hinton. From an engineering point of view a relative error in the range of 3% is always acceptable, especially, when the average error is only about 1%. Additional tests for meshes that are distorted so strongly that some quads degenerate to triangles with curved edges, show that the errors do not increase significantly. For more regular meshes, e.g. 3×3 elements with approximately parallel edges, the errors vanish with increasing regularity.

The results of the bending patch test are shown in Table 2. Again the relative errors are acceptable from an engineering point of view. It was found that the distorted mesh cannot meet the analytical solution for the transverse displacements in all integration points exactly. Only a nine-node element could be able to do this. With increasing thickness this error decreases due to the diminishing influence of the transverse orthogonality constraint on the deformation of the patch. Again, tests were made for meshes that are distorted so much that some quads degenerate to triangles with curved edges. It was found that the errors did not increase significantly. For regular meshes with approximately parallel element edges the errors vanish.

Next, the convergence of the linear solution due to mesh refinement is analysed considering the

Table 2
Bending patch test: maximum and averaged relative errors

Thickness: h	$\frac{\max \lvert\Delta E_{RI}\rvert}{E_{RI}}$	$\frac{\max \lvert\Delta E_{RII}\rvert}{E_{RI}}$	$\frac{\sqrt{\frac{1}{n}\sum_n \Delta E_{RI}^2}}{E_{RI}}$	$\frac{\sqrt{\frac{1}{n}\sum_n \Delta E_{RII}^2}}{E_{RI}}$
0.001	0.02485	0.02154	0.01233	0.01264
0.01	0.02320	0.02024	0.01163	0.01180
0.1	0.00368	0.00299	0.00186	0.00156

Analytical principal bending strains: $E_{RI} = 0.75 \cdot 10^{-3}$ h, $E_{RII} = 0.25 \cdot 10^{-3}$ h.

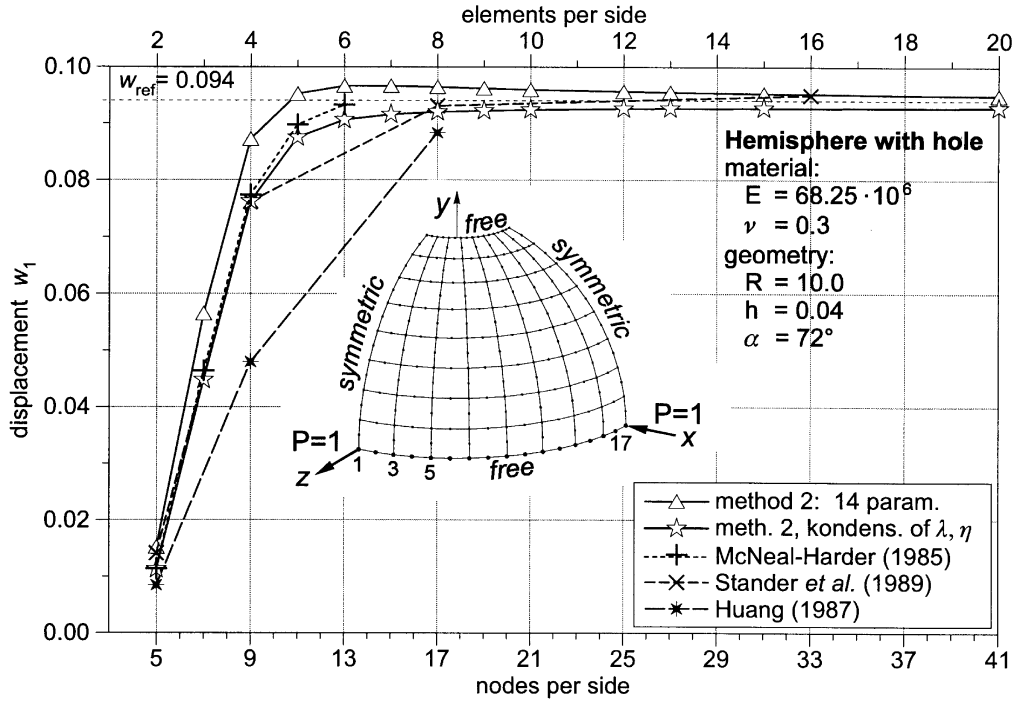

Fig. 4. Thin hemispherical shell with hole: convergence of the linear solution due to mesh refinement.

hemispherical shell with a hole, which has been investigated first by MacNeal and Harder (1985). The results are shown in Figs 4–9. In Fig. 4 the convergence of our finite element with the proposed assumed strain method 2 with 14 free parameters (see Section 6) is compared with the solutions published in MacNeal and Harder (1985) using the NASTRAN QUAD8 element with selective reduced integration, with the solutions according to Huang and Hinton (1986), Huang (1987a, b), and with the S08 shell element of Stander et al. (1989) with uniformly reduced integration. It is seen that our element shows a good performance also for relatively coarse meshes without and with condensation of the Lagrange multipliers λ and η. Solutions without stiffening effects also for extreme coarse meshes are known only for four-node elements.

In Fig. 5 the convergence behavior of the assumed strain technique implemented in the presented shell element is investigated. Our proposed assumed strain method 2 with 14 parameters seems to be the best one, followed by the Huang–Hinton method. Our proposed method 1 with 13 parameters shows comparable performance, for rather coarse meshes better, for medium coarse ones worse, but still better than the well-established Bathe–Dvorkin method. Solutions without applying any assumed strain or reduced integration methods have such weak convergence that they are not presented here.

In Fig. 6 the stiffening influence of condensation of the Lagrange multipliers is shown. It is seen that the slightly too weak solutions for medium coarse meshes appear only, if the Lagrange multipliers λ for the control of the normality of the directors are not condensed on element level. The reason is the fact that without condensation of λ the corresponding nodal degrees-of-freedom

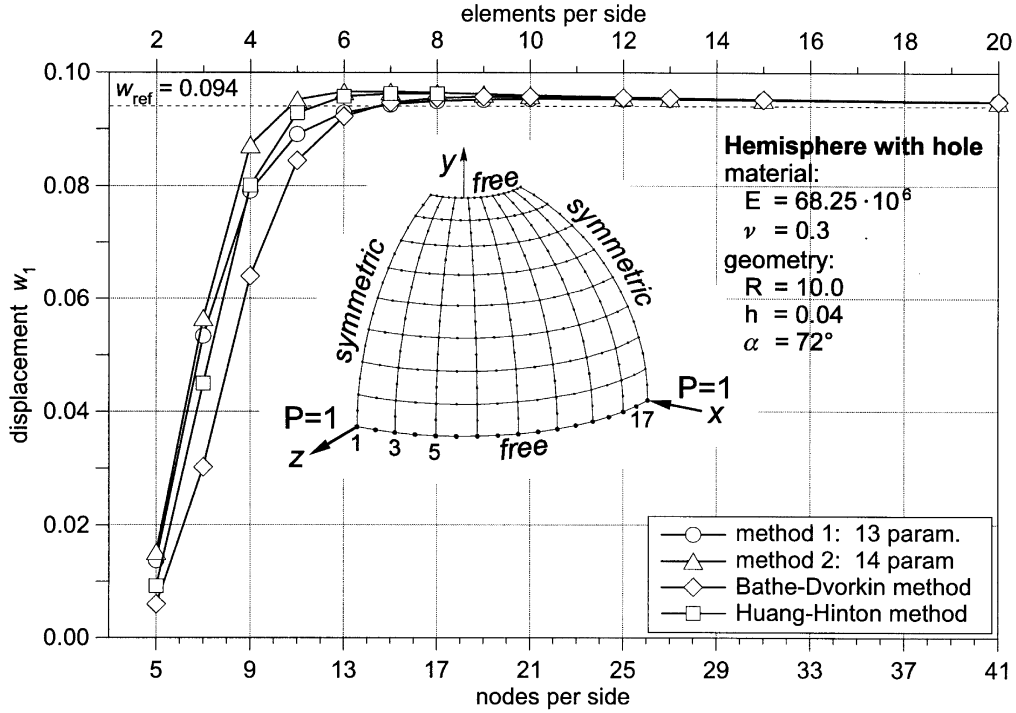

Fig. 5. Thin hemispherical shell with hole: convergence due to different assumed strain methods.

of λ are the same as those of neighboring elements, which is not the case, if condensation on element level is performed. Thus, with the condensation of λ the normality constraint of the directors is stronger enforced.

Figure 7 shows the convergence of mesh refinement for the nonlinear elastic–plastic analysis of the previous sample. Our proposed assumed strain method 2 without condensation was always applied. The need of finer meshes than 8×8 for larger deformations is mainly required by the strong bending effects near the loading points 1 and 2. Measurements of the mean curvatures and estimations of the characteristic wave lengths of boundary bending effects there give an advice for the reliable maximal element size at these places. One should take into account that an eight-node C^0 finite shell element can represent typically only bi-linear distributions of the bending moment. Therefore, optimal low-cost performance can be achieved with non-uniform meshes, which are refined at the boundaries and in the regions of strong bending. In the case of too coarse meshes the strain distributions across the element boundaries will lead to jumps. But in this case the mesh is always too coarse to be able to represent appropriately the boundary bending effects, because from the engineering point-of-view one needs at least two elements for one half of the characteristic wave length. This fact is well known in the applications of finite shell elements.

In Figs 8 and 9 the influence of a decreasing ratio of shell thickness to radius h/R on the mesh convergence is represented. The corresponding geometry and boundary conditions are shown in Figs 4 and 5, only the thickness is altered. The dimensionless linear solutions for various meshes using the proposed assumed strain method 2 with 14 parameters without and with condensation

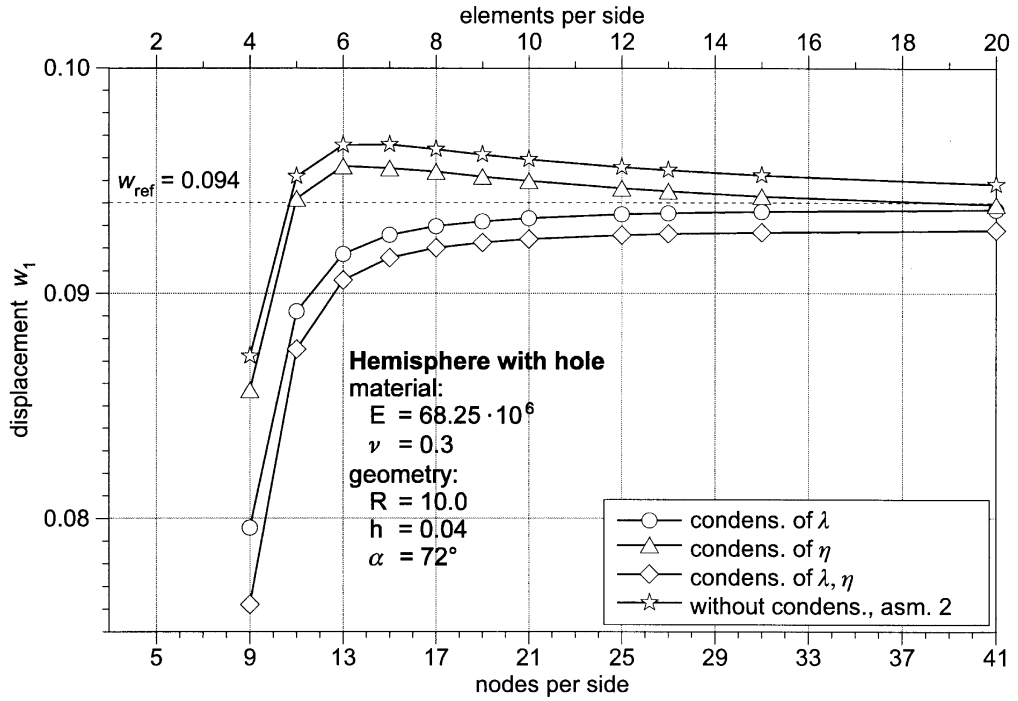

Fig. 6. Thin hemispherical shell with hole: influence of the Lagrange multiplier condensation on the convergence.

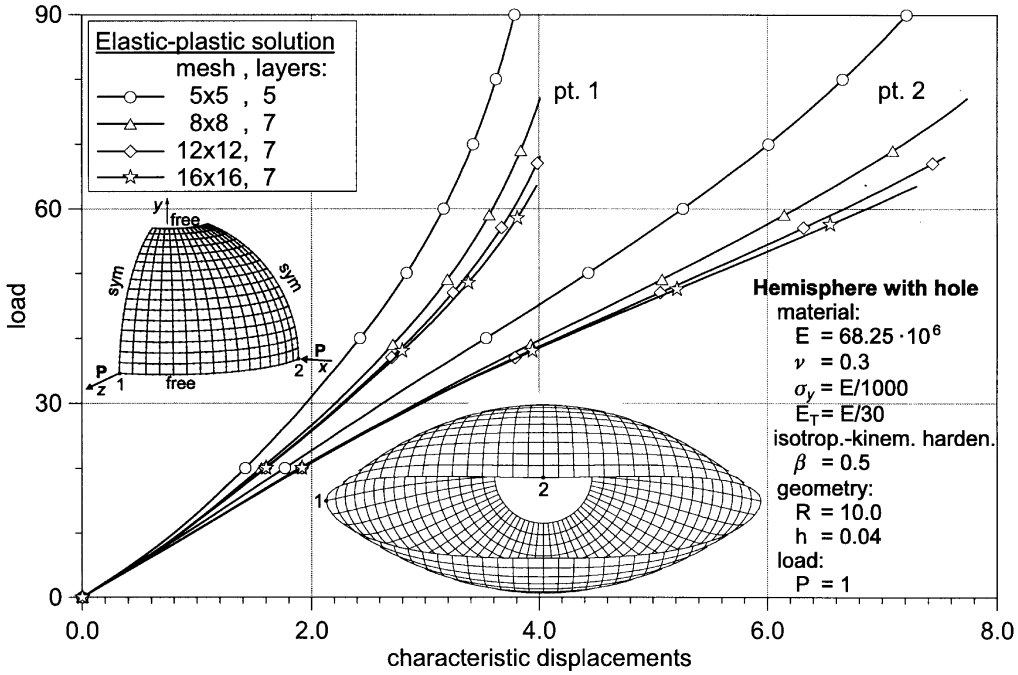

Fig. 7. Thin hemispherical shell with hole: elastic–plastic solutions.

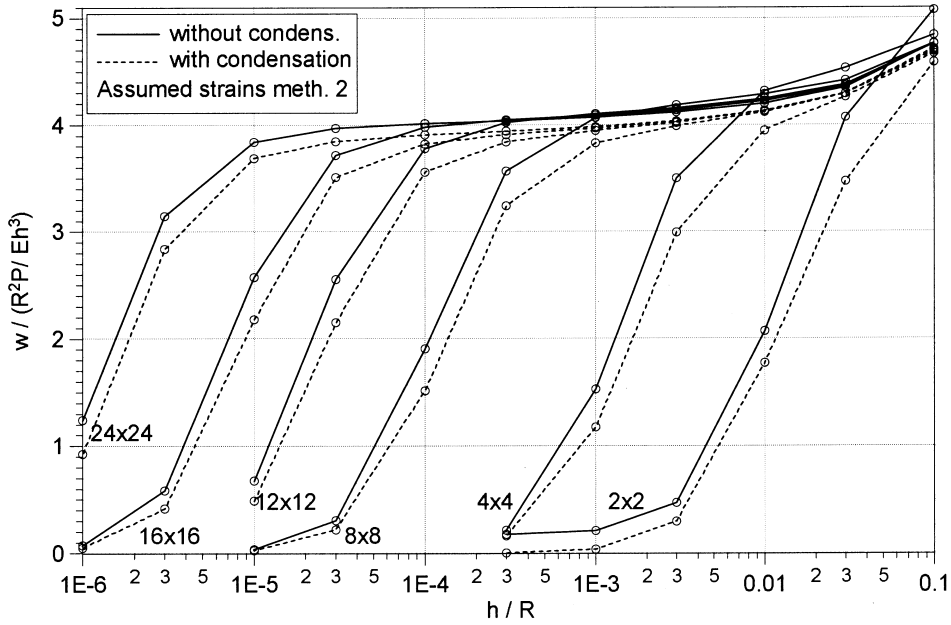

Fig. 8. Thin hemispherical shell with hole: linear solutions of various meshes for decreasing thickness.

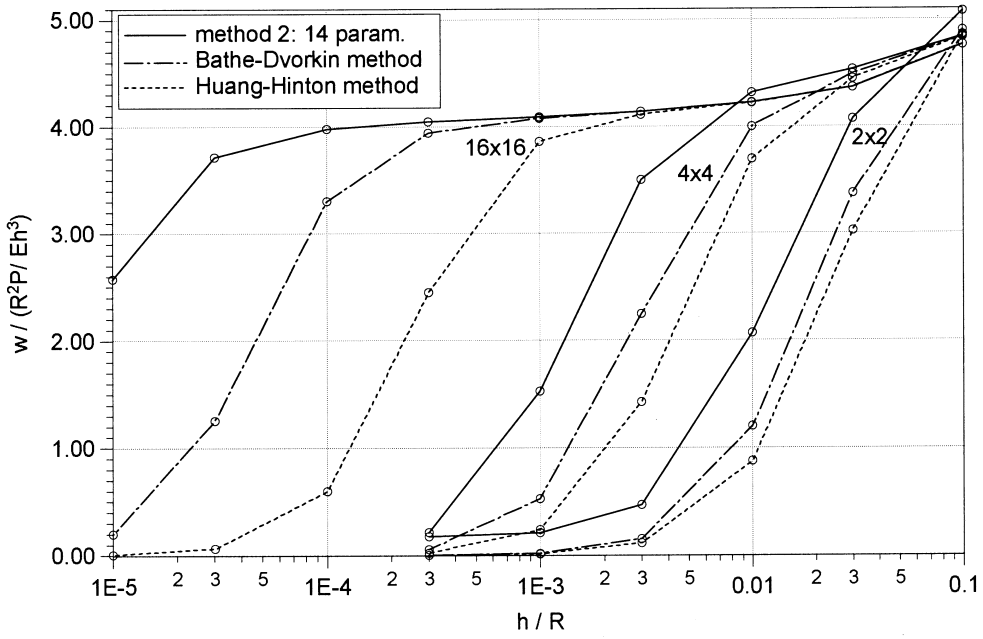

Fig. 9. Thin hemispherical shell with hole: linear solutions of different assumed strain methods for decreasing thickness.

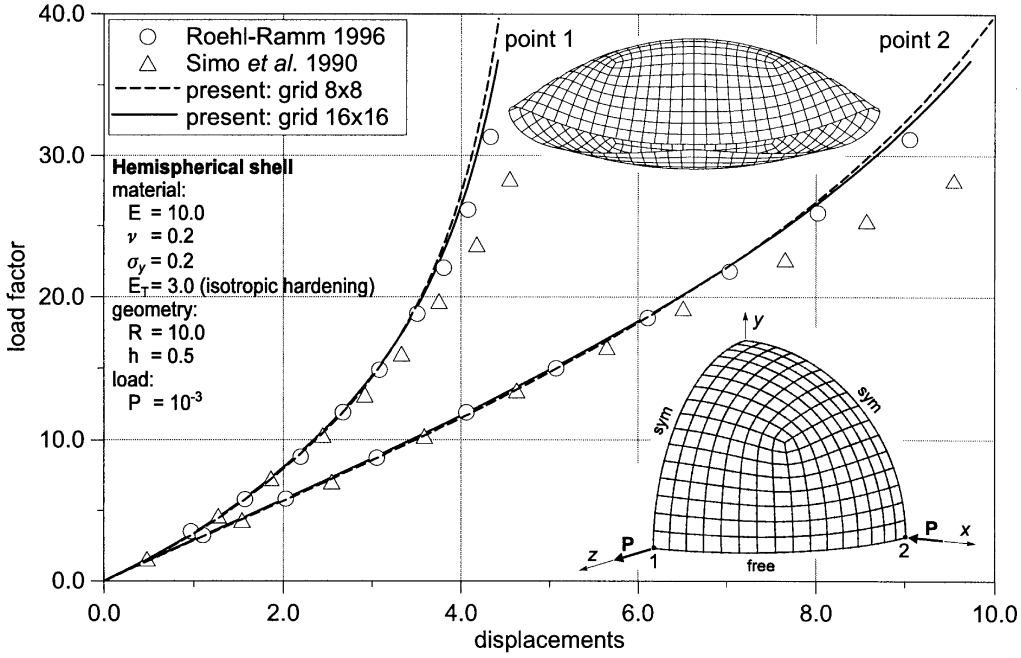

Fig. 10. Moderately thin hemisphere: elastic–plastic analysis.

of Lagrange multipliers are shown in Fig. 8. One recognizes that a reduction of the relative thickness by the factor 10 needs a mesh refinement of factor 2 in each direction. In Fig. 9 the dimensionless linear solutions for the proposed assumed strain method 2 with 14 parameters, for the Bathe–Dvorkin and for the Huang–Hinton method are shown using three different meshes with 2×2, 4×4 and 16×16 elements. One can easily recognize that the method proposed in the present paper has the best performance.

The last sample shown in Fig. 10 is the elastic–plastic analysis of the moderately thin hemisphere of Simo (1990). As in the previous example, only small strains occur due to the thinness of the shell. Because of the increased thickness ($h/R = 0.05$ instead of 0.004 previously), the characteristic wave length is increased as well, and even the 8×8 mesh produces nicely converging results. They confirm the results of the six-parameter shell element and the full three-dimensional analysis of Roehl and Ramm (1996). However, the solutions of Simo (1990) seem to be too soft for larger deformations.

Additionally, the results of a comprehensive set of numerical examples accounting also for finite elastic–plastic strains with anisotropies and strain localization will be presented in Part II of this paper.

Acknowledgement

The authors gratefully acknowledge financial support of the Deutsche Forschungsgemeinschaft (DFG) under Contract No. ST-135/2.

References

An, Q., Kollmann, F.G., 1996. A general theory of finite deformation of viscoplastic thin shells. Acta Mech. 117, 47–70.

Başar, Y., Ding, Y., 1990. Finite-rotation elements for the non-linear analysis of thin shell structures. Int. J. Solids Structures 26, 83–97.

Başar, Y., Ding, Y., 1997. Shear deformation models for large strain shell analysis. Int. J. Solids Structures 34 (14), 1687–1708.

Başar, Y., Ding, Y., Krätzig, W.B., 1992. Finite-rotation shell elements via mixed formulation. Computational Mechanics 10, 289–306.

Başar, Y., Krätzig, W., 1989. A consistent shell theory for finite deformations. Acta Mech. 76, 73–87.

Başar, Y., Weichert, D., 1991. A finite-rotation theory for elastic–plastic shells under consideration of shear deformations. ZAMM 71, 379–389.

Bathe, K.J., Dvorkin, E.M., 1986. A formulation of general shell elements, the use of mixed interpolation of tensorial components. Int. J. Num. Meth. Engng 22, 697–722.

Bilby, B.A., Bullough, R., Smith, E., 1955. Continuous distributions of dislocations: a new application of the methods of non-Riemannian geometry. Proc. Roy. Soc. London A231, 263–273.

Brank, B., Perić, D., Damjanic, F., 1997. On large deformations of thin elasto-plastic shells: implementation of a finite rotation model for quadrilateral shell element. Int. J. Num. Meth. Engng 40, 689–726.

Büchter, N., Ramm, E., 1992. Shell theory versus degeneration—a comparison in large rotation finite element analysis. Int. J. Num. Meth. Engng 43, 39–61.

Büchter, N., Ramm, E., Roehl, D., 1994. Three-dimensional extension of nonlinear shell formulation based on the enhanced assumed strain concept. Int. J. Num. Meth. Engng 37, 2551–2568.

Chroscielewski, J., Makowski, J., Stumpf, H., 1992. Genuinely resultant shell finite elements accounting for geometric and material nonlinearity. Int. J. Num. Meth. Engng 35, 63–94.

Chroscielewski, J., Makowski, J., Stumpf, H., 1997. Finite element analysis of smooth, folded and multi-shell structures. Comp. Meth. Appl. Mech. Engng 141, 1–46.

Gruttmann, F., Stein, E., Wriggers, P., 1989. Theory and numerics of thin elastic shells with finite rotations. Ing. Arch. 59, 54–67.

Huang, H.C., 1987a. Implementation of assumed strain degenerated shell elements. Comp. Struct. 25, 147–155.

Huang, H.C., 1987b. Membrane locking and assumed strain elements. Comp. Struct. 27, 671–677.

Huang, H.C., Hinton, E., 1986. A nine node degenerated shell element with enhanced membrane and shear interpolation. Int. J. Num. Meth. Engng 22, 73–92.

Kröner, E., 1960. Allgemeine Kontinuumstheorie der Versetzungen und Eigenspannungen. Arch. Rat. Mech. Anal. 4, 273–334.

Le, K.C., Stumpf, H., 1993. Constitutive equations for elastoplastic bodies at finite strain: thermodynamic implementation. Acta Mechanica 100, 155–170.

Lee, E.H., 1969. Elasto-plastic deformation at finite strains. J. Appl. Mech. 36, 1–6.

MacNeal, R.H., Harder, R.L., 1985. A proposed standard set of problems to test finite element accuracy. Finite Elements in Analysis and Design 1, 3–20.

Makowski, J., Stumpf, H., 1989. Finite axisymmetric deformation of shells of revolution with application to flexural buckling of circular plates. Ing.-Arch. 39, 456–472.

Makowski, J., Stumpf, H., 1990. Buckling equations of elastic shells with rotational degrees of freedom undergoing finite strain deformation. Int. J. Solids Structures 26, 353–368.

Miehe, C., 1998a. A constitutive frame of elastoplasticity at large strains based on the notion of a plastic metric. Int. J. Solids Structures 35 (30), 3859–3897.

Miehe, C., 1998b. A theoretical and computational model for isotropic elasto-plastic stress analysis in shells at large strains. Comp. Meth. Appl. Mech. Engng 155, 193–233.

Nolte, L.-P., Makowski, J., Stumpf, H., 1986. On the derivation and comparative analysis of large rotation shell theories. Ing.-Arch. 56, 145–160.

Ogden, R.W., 1984. On Eulerian and Lagrangian objectivity in continuum mechanics. Arch. Mech. Stos. 36, 297–218.

Pietraszkiewicz, W., 1984. Lagrangian description and incremental formulation in the non-linear theory of thin shells. Int. J. Non-Linear Mech. 19, 115–140.

Pietraszkiewicz, W., 1989. Geometrically nonlinear theories of thin elastic shells. Adv. Mech. 12, 51–130.

Roehl, D., Ramm, E., 1996. Large elasto-plastic finite element analysis of solids and shells with the enhanced assumed strain concept. Int. J. Solids Structures 33 (20-22), 3215–3237.

Rouainia, M., Perić, D., 1998. A computational model for elasto-viscoplastic solids at finite strain with reference to thin shell applications. Int. J. Num. Meth. Engng 42, 289–311.

Sansour, C., Bufler, H., 1992. An exact finite rotation shell theory, its mixed variational formulation and its finite element implementation. Int. J. Num. Meth. Engng 34, 73–115.

Schieck, B., Pietraszkiewicz, W., Stumpf, H., 1992. Theory and numerical analysis of shells undergoing large elastic strains. Int. J. Solids Structures 29 (6), 689–709.

Schieck, B., Stumpf, H., 1993. Deformation analysis for finite elastic–plastic strains in a Lagrangian-type description. Int. J. Solids Structures 30 (19), 2639–2660.

Schieck, B., Stumpf, H., 1995. The appropriate corotational rate, exact formula for the plastic spin and constitutive model for finite elasto-plasticity. Int. J. Solids Structures 32 (24), 3643–3667.

Schmidt, R., Weichert, D., 1989. A refined theory of elastic–plastic shells at moderate rotations. ZAMM 69, 11–21.

Simmonds, J. G., 1985. The strain energy density of rubber-like shells. Int. J. Solids Structures 21, 67–77.

Simmonds, J. G., 1986. The strain energy density of rubber-like shells of revolution undergoing torsionless, axisymmetric deformation (axishells). J. Appl. Mech. 53, 593–596.

Simo, J.C., 1988. A framework for finite strain elastoplasticity based on maximum plastic dissipation and multiplicative decomposition: Part I, Continuum formulation. Comp. Meth. Appl. Mech. Engng 66, 199–219.

Simo, J.C., Fox, D.D., 1989. On a stress resultant geometrically exact shell model. Part I: Formulation and optimal parametrization. Comp. Methods Appl. Mech. Engng 72, 267–304.

Simo, J.C., Kennedy, J.G., 1992. On a stress resultant geometrically exact shell model. Part V: Nonlinear plasticity: formulation and integration algorithms. Comp. Meth. Appl. Mech. Engng 96, 133–171.

Simo, J.C., Ortiz, M., 1985. A unified approach to finite deformation elastoplastic analysis based on the use of hyperelastic constitutive equations. Comp. Methods Appl. Mech. Engng 49, 221–245.

Simo, J.C., Rifai, M.S., Fox, D.D., 1990. On a stress resultant geometrically exact shell model. Part IV: Variable thickness shells with through the thickness stretching. Comp. Meth. Appl. Mech. Engng 81, 91–126.

Stander, N., Matzenmiller, A., Ramm, E., 1989. An assessment on assumed strain methods in finite rotation shell analysis. Engng Comp. 3 (3), 58–66.

Stumpf, H., Makowski, J., 1986. On large strain deformation of shells. Acta Mech. 45, 153–168.

Stumpf, H., Schieck, B., 1994. Theory and analysis of shells undergoing finite elastic–plastic strains and rotations. Acta Mechanica 106, 1–21.

Valid, R., 1986. Finite rotations, variational principles and buckling in shell theory. In: Pietraszkiewicz, W. (Ed.), Finite Rotations in Structural Mechanics. Springer Verlag, Berlin, Heidelberg, New York, Tokyo, pp. 317–312.